The Logic of Change: Contextual Adaptation of a Mobile Gene

Nathan Grassi

A dissertation

submitted in partial fulfillment of the

requirements for the degree of

Doctor of Philosophy

University of Washington

2025

Reading Committee:

Benjamin Kerr, Chair

Neda Bagheri

Daniel Promislow

Program Authorized to Offer Degree:

Department of Biology

University of Washington

Abstract

The Logic of Change: Contextual Adaptation of a Mobile Gene

Nathan Grassi

Chair of the Supervisory Committee:
Benjamin Kerr
Department of Biology

Understanding how genotypes map to fitness is fundamental to the description and prediction of adaptive evolution. Through differential reproductive fitness of heritable variation, populations enhance survival and reproduction within the selective environment. In this dissertation, I employ experimental evolution of cefotaxime resistance in the plasmid-encoded *bla*$_{\text{TEM}}$ with selection occurring in two bacterial species that host this gene. I measure resistance phenotype during the evolution experiment and utilize monoculture barcoded fitness assays to evaluate the competitive ability of numerous plasmid genotypes hosted by the same species in a range of antibiotic environments. I introduce the concept of an adaptive window to delineate the region of concentration space where each sampled mutation would be selectively accessible in each species. We observe that resistance effects

of mutations often correlate between species, but the window of selective accessibility is shifted between species due to differences in intrinsic resistance level. In Chapter 2, I perform side-by-side monoculture and coculture barcoded fitness assays to evaluate the competitive ability of plasmid-host pairings across distinct host communities. We observe that both plasmid genotypic fitness and the fitness effect of mutations can depend strongly on host community structure. Together, these chapters demonstrate that the ecology and evolution of mobile genetic elements can be shaped by host genomic and host community contexts. More generally, this dissertation highlights the dynamic nature of the genotype-to-fitness mapping which is modulated by contextual factors ranging from within the gene, cell, or ecosystem.

Introduction

The evolution of mobile antibiotic resistance genes is shaped not only by selection for resistance, but also by the ecological contexts in which that selection occurs. My dissertation examines how ecological and evolutionary context determine the adaptive trajectory of the *bla*$_{TEM}$ gene, which encodes a beta lactamase protein that hydrolytically inactivates beta lactam antibiotics. Building on prior work examining plasmid-mediated resistance across bacterial hosts, I apply a directed evolution framework to interrogate how resistance-enhancing mutations arise and persist in *Escherichia coli* and *Klebsiella pneumoniae*. By selecting for increased cefotaxime resistance in both species, I evaluate whether the selective consequences of individual mutational steps are conserved across hosts and antibiotic environments.

This work is novel in that selection during directed evolution is applied in multiple host species. Furthermore, we evaluate mutational effect in bulk fitness competitions of genetically reconstructed genotypes within each host species across numerous antibiotic environments. I introduce the concept of an "adaptive window" to describe the specific environments in which a resistance mutation confers a fitness advantage. While overall resistance phenotypes are often similar between species, the adaptive windows of mutations vary, revealing context-dependent constraints on mutational accessibility. These results suggest that although the identity of many resistance mutations are shared between species, their evolutionary accessibility is shaped by host-specific ecological factors.

In the second part of my dissertation, I quantify how plasmid evolution changes in the presence of multiple hosts. Appending a coculture treatment to the barcoded fitness assay employed in Chapter 1, I measure plasmid genotype fitness and mutation effects in single and multispecies bacterial communities. We find that *E. coli*-harbored plasmids grow much slower in coculture relative to monoculture, while the impact *K. pneumoniae* genotypes is much less severe. Importantly, we observe shifts in the fitness effects of mutations across conditions, indicating that interspecies interactions reshape the selective landscape. These findings demonstrate that the ecology and evolution of mobile genetic elements are shaped by the interaction between host genotype and community structure.

Chapter 1

Through the Adaptive Window and What Contexts Modulate the Fitness Landscape

Nathan Grassi, Fischer Tsai, Benjamin Kerr

Abstract

The fitness effect of mutations can vary across genetic or environmental contexts, potentially yielding divergent evolutionary outcomes. We combine directed evolution of a mobile antibiotic resistance gene with high-throughput barcoded plasmid fitness competitions to generate reaction norms depicting the fitness effect selected mutations across antibiotic and host backgrounds. We find that while resistance effects tend to correlate between species, the region of concentration space where this benefit was realized (i.e., the *adaptive window)* often varied between our two host species. Moreover, we identify mutational steps that exhibit idiosyncratic species-specific fitness effects, wherein the same mutation on the same genetic background confers a benefit in one species but not another. Our results suggest that multidimensional selective forces shape the accessibility of evolutionary trajectories in mobile genes and highlight the importance of direct fitness measures across interacting layers of context to improve prediction of eco-evolutionary phenomena in complex adaptive systems.

Introduction

In Lewis Carroll's imagined worlds, stepping across a threshold does more than reveal a new view — it rearranges the rules of space itself. In evolution, a similar shifting of rules occurs as the effect of mutations is reframed by changes in ecological or genetic context. Adaptive landscapes, mappings of genotype-to-fitness within a selective context, are not static terrains but shifting spaces wherein the same genetic change that is advantageous under certain selective conditions might be neutral or even harmful to fitness elsewhere.[1–16] The fitness effect of mutations can be influenced by multiple layers of context: interactions with other genetic loci,[13,17–27] the host background,[24,28–35] and the environment.[1,36–41] Predicting the course of adaptive evolution requires a framework that accounts for modulation of mutational effect across relevant contextual dimensions.[4,9,10,42–45] Mutation reaction norms provide a useful framework for examining the phenotypic effect of a mutation across selective contexts.[16,46] Furthermore, when the measured phenotype is competitive fitness, these reaction norms can demonstrate the contexts where mutant types have a competitive advantage relative to their ancestor.

Antibiotic resistance, as a rule, does not come for free.[40,47–55] Frequently, the fitness advantage of a resistance mutation is contingent on the presence and concentration of the relevant antibiotic.[49,53,54,56,57] Resistance mutations in plasmid-encoded beta lactamase, *bla*$_{\text{TEM}}$, often carry collateral fitness costs that reduce bacterial fitness in the absence of beta lactam drugs.[39,46,48,49,55,58] At low drug levels, wildtype or low-resistance genotypes may outcompete resistant mutants.[39,50,55,58,59] This results in an adaptive window: a specific range of factor space (e.g., antibiotic concentration) where a mutation confers a fitness benefit.[53,57,58] Below this window, the mutant's fitness cost outweighs the resistance advantage. Within the window, there is a net fitness advantage where the mutant survives while the ancestor is inhibited until eventually a concentration is reached that inhibits both types. Mapping these adaptive windows allows us to define the context within which mutations are accessible to natural selection.

In this study, we applied this framework to investigate how mutations in the mobile *bla*$_{\text{TEM}}$ gene shape cefotaxime resistance across two bacterial host species, *Escherichia coli* and *Klebsiella pneumoniae*. We conducted a directed evolution (DE) experiment to select for cefotaxime resistance mutations in *E. coli* and *K. pneumoniae*, allowing adaptive mutations to accumulate under increasing antibiotic pressure. To quantify the fitness effects of these

mutations across species and selective conditions, we reconstructed single-step substitutions and evaluated their fitness in competition across a gradient of cefotaxime concentrations. Our results reveal that while resistance mutations in *bla*$_{TEM}$ generally confer a fitness benefit across species, the specific environments where they are selectively accessible vary. The primary resistance mutation G238S emerged as the dominant substitution in both species, consistent with its well-documented role in cefotaxime resistance.[25,60–62] However, certain mutational combinations demonstrated species-specific fitness effects, suggesting that host-intrinsic factors can influence the accessibility of mutational trajectories. Our findings corroborate our previous work[24] that the global structure of the resistance landscape is largely conserved but show that species-specific selection pressures shape the precise evolutionary paths and environments comprising the adaptive window for resistance mutations.

Experimental Approach

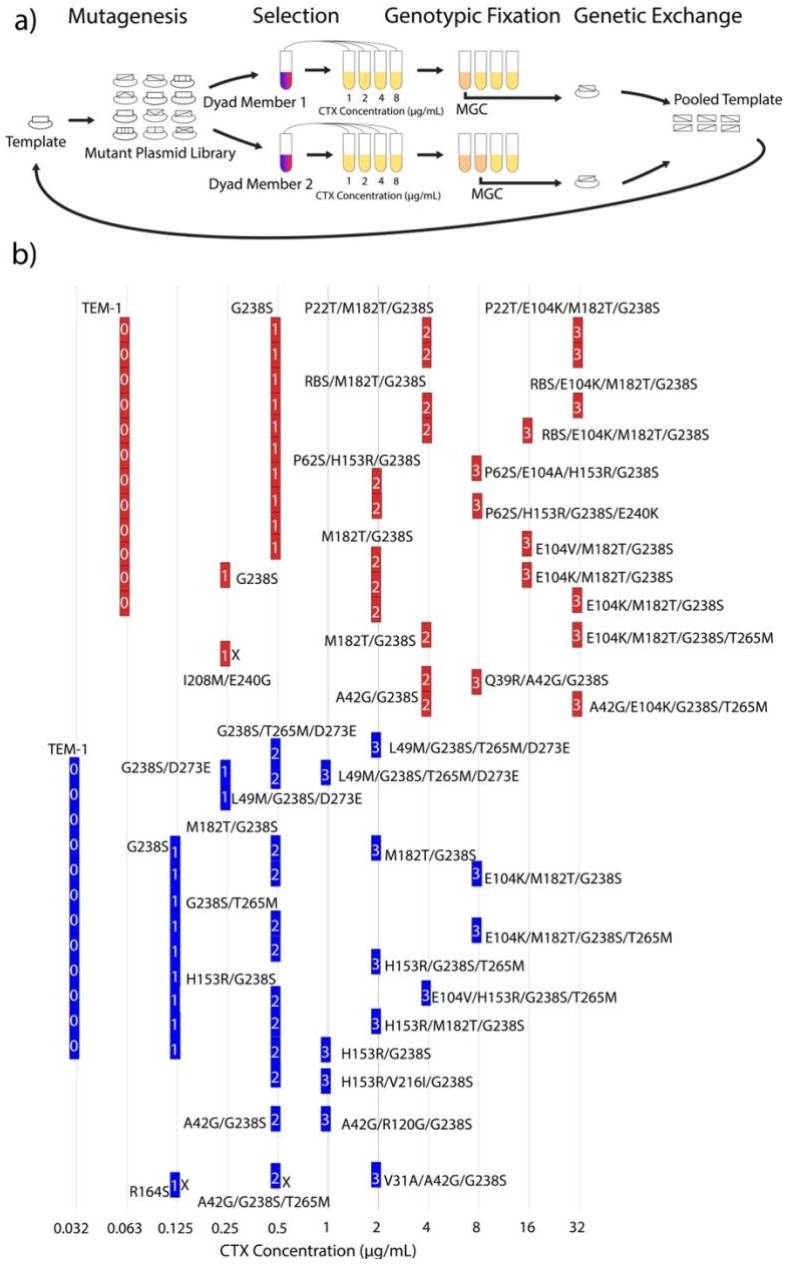

Figure 1. a) Workflow for the directed evolution (DE) experiment. Beginning with TEM-1 plasmid template, the gene is mutagenized in 12 independent error-prone polymerase chain reactions. Each mutant library is transformed into a pair/dyad of bacterial populations with four dyads consisting of two populations of *E. coli,* four dyads of two populations of *K. pneumoniae*, and four dyads with a single population of each species. Dyad populations are inoculated along cefotaxime gradients and incubated for 20 hours. The plasmid is then isolated from a random clone from the culture at the highest concentration to exhibit turbidity (referred to as the maximum growth concentration, MGC). Conventional PCR is used to amplify the gene for Sanger sequencing then PCR products from the two dyad members belonging to the same evolution line are mixed equally to serve as template for the next round of error-prone PCR. b) Genotypes from the DE experiment are reported at the MGC they were selected each round. Bars are colored according to the species that the genotype was selected in (*E. coli* in red; *K. pneumoniae* in blue) and labeled with the round selected. Genotypes that were subsequently replaced by mutational steps on the genotypic background fixed in the other dyad member are shown with X's.

Selection for *de novo* resistance mutations occurred in 12 populations of each species through 3 rounds of DE (Fig. 1a). All 12 populations within each species began as the wildtype, TEM-1 with no designated resistance mutations. Due to intrinsic resistance differences between species, this same plasmid genotype can survive at a higher concentration when hosted by *E. coli* relative to *K. pneumoniae*. In the first round, both species frequently substituted G238S, which eventually appeared in every evolutionary endpoint (Fig. 1b). Although other mutations were selected in the first round (R164S in *K. pneumoniae;* and I208M/E240G in *E. coli*), both dyad members the next round fixed a mutational step on the G238S background that was fixed in the other dyad member belonging to the same evolution line (Extended Data Fig. 1). R164S is a well-documented resistance mutation, but this substitution is known to interact negatively with G238S[25,58,60,63], which precluded the selection the R164S/G238S double mutant. Both the I208M and E240G substitutions have been isolated in previous directed evolution studies and are associated with effects on enzyme stability and hydrolysis; respectively,[60,63] but their combined resistance effect was outpaced by G238S alone. The most resistant *K. pneumoniae* dyad members of the first round fixed the double mutant, G238S/D273E, which we confirmed increased resistance in *K. pneumoniae* over G238S alone but does not detectably affect resistance in *E. coli* (Extended Data Fig. 2).

In the second round, many populations acquired mutations that appeared to mitigate the collateral fitness effects of the destabilized, albeit more resistant, mutant enzyme. The M182T substitution, known to be a global suppressor of destabilizing mutational effects associated with other loci, was utilized by both species but at a higher frequency by *E. coli* whereas *K. pneumoniae* more often selected stabilizing mutations H153R and T265M alongside M182T.[60,63] In combination with M182T, *E. coli* dyad members sampled a nucleotide change in the upstream ribosome binding site (RBS)[64] and the P22T amino acid substitution in the periplasmic signal, both of which putatively affect expression and localization of the mature protein.[48] The A42G substitution appeared in both species and is known to interact positively with G238S, while the L49M and P62S substitutions also appeared in *K. pneumoniae* and *E. coli;* respectively, and both are associated with a stabilizing effect.[60,63]

In the third round, highly resistant genotypes incorporated additional resistance mutations at residues E104 and E240, both known to affect substrate specificity. [60,63] In *E. coli*, E104K and E104V were acquired to genetics background containing M182T while E104A and E240K were acquired on backgrounds stabilized by H153R (in combination with additional stabilizing substitution, P62S). In *K. pneumoniae*, E104K occurred with M182T and E104V occurred with H153R (in combination with an additional compensatory mutation, T265M). More moderate increases in resistance were observed for genotypes that further combined compensatory mutations including V31A, R120G, V216I. [60,63] To better understand how each mutation contributed to resistance and fitness in different host backgrounds, we reconstructed each single-step intermediate genotype from the DE experiment using site-directed mutagenesis. Each genotype was barcoded in triplicate to allow for precise tracking of fitness in bulk competitions across a gradient of cefotaxime concentrations independently in *E. coli* and *K. pneumoniae* (Figure 2a).

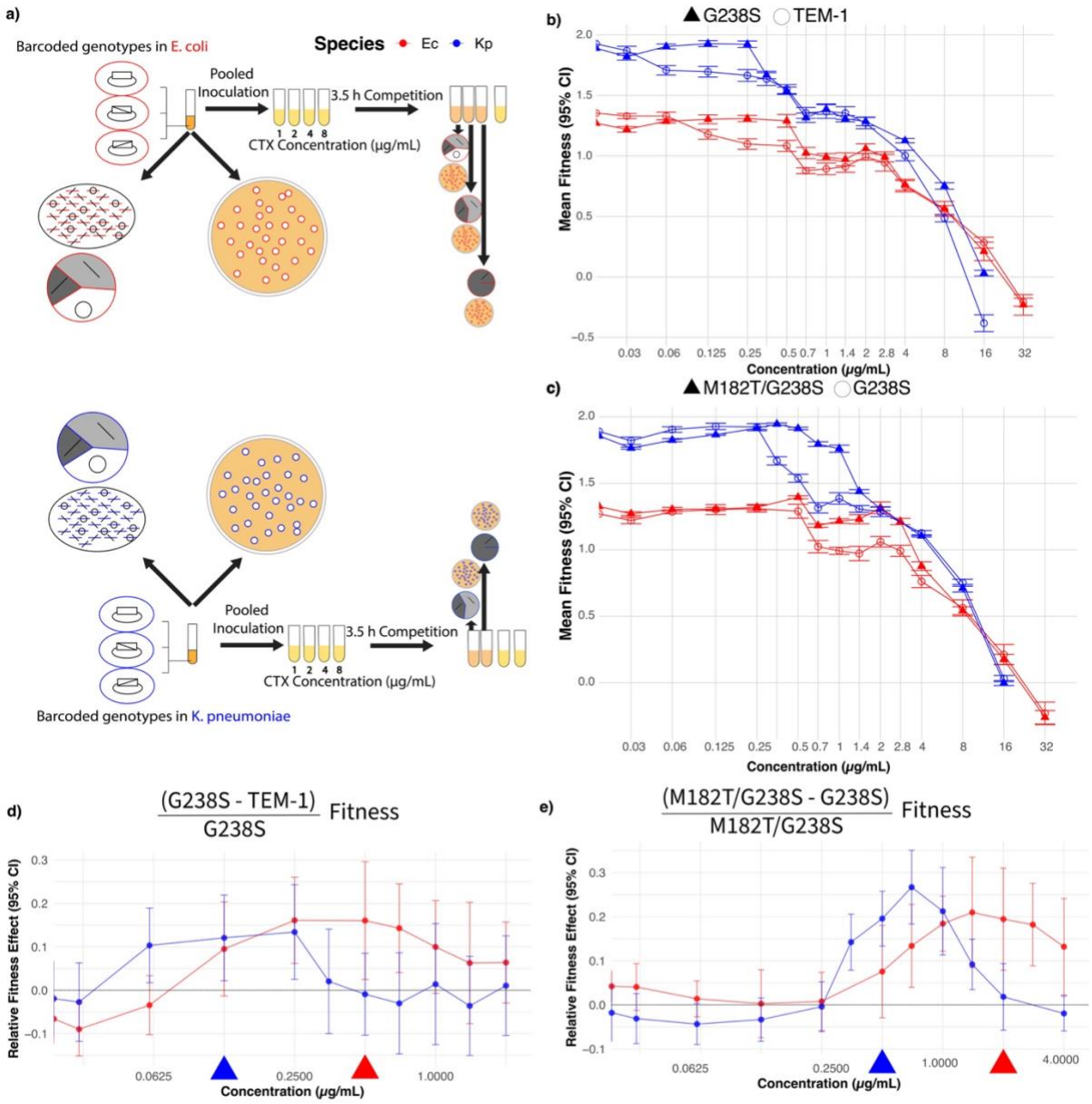

Figure 2. a) Workflow for the barcoded fitness assay. Each plasmid genotype has replicate barcode sequences transformed into naive cells of *E. coli* and *K. pneumoniae.* Amplicon sequencing of the barcode region and selective plating are used to estimate initial genotype frequencies and culture density in separate species monocultures. These species cultures are inoculated across separate antibiotic gradients and genotypes are competed for 3.5 hours. Final barcode frequencies and cell densities are estimated from each tube. b-c) Genotypic fitness with 95% confidence intervals as a function of antibiotic concentration for mutationally-adjacent ancestor (open circles) and mutant neighbor genotypes (filled triangles) in *E. coli* (red) and *K. pneumoniae* (blue). d-e) Mutational effect is calculated through an evaluation of the relative fitness difference of mutant neighbors [(Mutant Fitness – Original Fitness) / Mutant Fitness] in each tested antibiotic environment in both species. Error bars represent the 95% confidence interval of this relative fitness effect. e-f) Genotypic networks of mutational steps selected in *E. coli* and *K. pneumoniae;* respectively, during the DE experiment.

From the fitness competitions we observe the existence of a resistance-competitive ability trade-off between the two species with *E. coli* possessing a higher resistance but slower baseline growth rate (Fig. 2b-c). Consequently, the fitness of the same genotype is higher in *K. pneumoniae* than it is in *E. coli* (compare blue to red open circles, or blue to red filled triangles), suggesting that this species possesses a higher maximal growth rate over 3.5 h. However, these genotypes in *E. coli* exhibit a positive fitness at higher concentrations as compared to *K. pneumoniae*, consistent with the higher intrinsic resistance level of this species. When comparing fitness of different genotypes within the same species (compare blue or red open circle to blue or red filled triangles) we observe a similar resistance-competitive ability trade-off where the cost of resistance mutations prevents the selective advantage over the immediate ancestor in low-drug environments. However, this cost is offset by the benefit of enhanced drug resistance, which at some point sufficiently inhibits the ancestral type to render the mutation selectively accessible.

To determine which antibiotic concentrations resistance mutations are advantageous to each species, we evaluate the relative fitness effect of selected mutation in each species across the antibiotic gradient (Fig. 2d-e). These mutation effect reaction norms enable us to define adaptive window as the range of antibiotic environments where the fitness effect of a mutation is significantly positive (i.e., 95% CI of mutational effect is positive and does not contain 0). The mutation reaction norms for the G238S and M182T substitutions in the TEM-1 and G238S backgrounds; respectively, show an adaptive window where the mutation is associated with a positive fitness difference. Notably, the concentrations where each mutant genotype appeared during the DE experiment were situated within the adaptive window detected in our barcoded fitness assay, showing correspondence across experiments.

In the DE experiment, identical mutational steps were selected in each species but appeared in lower drug concentrations in *K. pneumoniae* compared to *E. coli*. Likewise, in the barcoded fitness assay, we observe that the same plasmid mutation confers a significant beneficial effect in lower drug concentrations for *K. pneumoniae* as compared to *E. coli*. The lower intrinsic resistance level of the *K. pneumoniae* host necessitates the acquisition of resistance mutations in the mobile gene earlier in concentration space as compared to the *E. coli* host background. Despite the substitution of similar resistance mutations in DE populations of *E. coli* and *K. pneumoniae,* we find that within the selected antibiotic environment that these mutations appear they often do not confer significant benefit to the other host background (Figure 3).

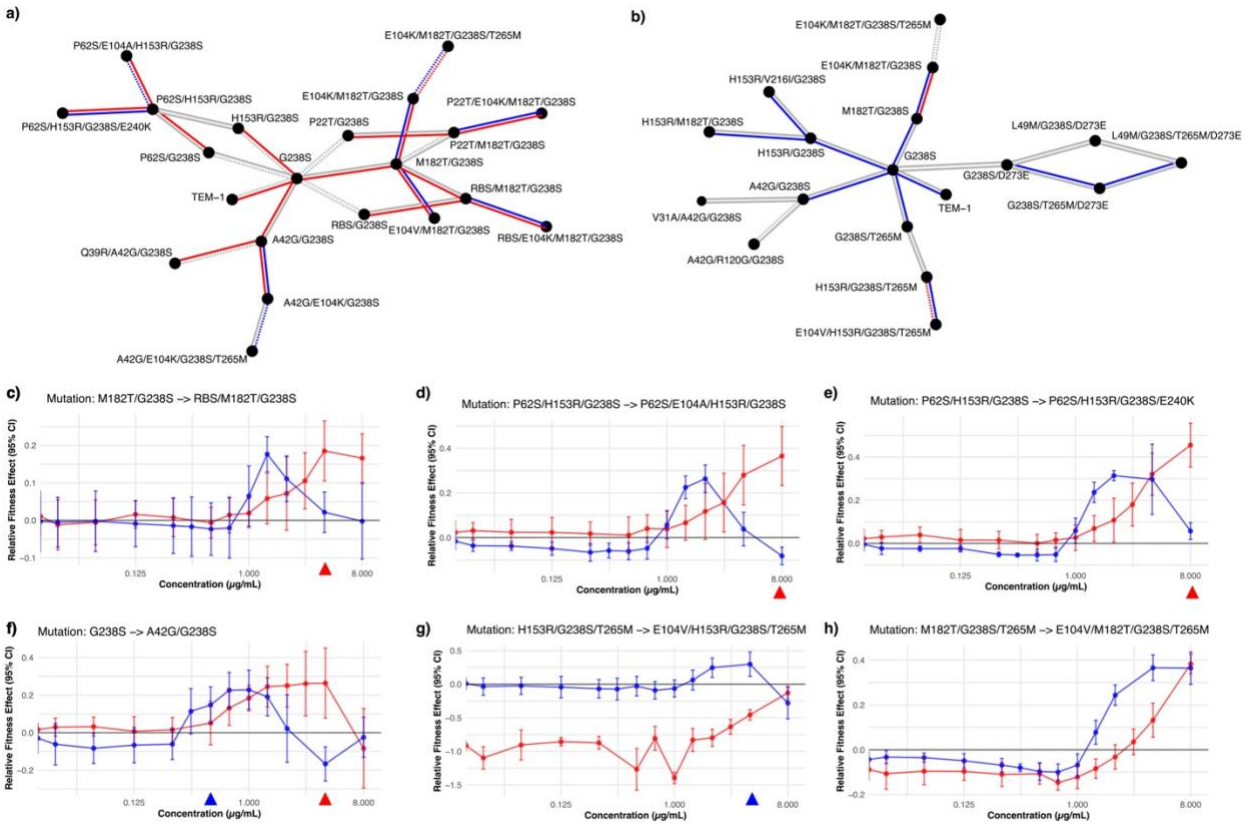

Figure 3. a) Genotypic network of mutational steps selected in *E. coli* dyad members during the DE experiment. Edges represent the scaled mutational effect in *E. coli* and *K. pneumoniae* hosts evaluated within antibiotic concentration that the mutant genotype was sampled in *E. coli* during the DE experiment. Edges between genotypes represent the relative fitness difference between mutant neighbor genotypes in the concentration that the mutation was selected in during the DE experiment. Edge color represents significant effect in *E. coli* (red) or *K. pneumoniae* (blue) and edge type represents mutational effect (positive, solid; negative, dashed). b) Genotypic network of mutational steps selected in *K. pneumoniae* dyad members during the DE experiment. Edges represent the scaled mutational effect in *E. coli* and *K. pneumoniae* hosts evaluated within antibiotic concentration that the mutant genotype was sampled in *K. pneumoniae* during the DE experiment. Same edge labeling as in panel a. c-e) Mutation effect reaction norms derived from the barcoded fitness assay are depicted with triangles denoting the concentration where the mutant genotypes were selected during the DE experiment in *E. coli* (red) and/or *K. pneumoniae* (blue).

Most mutations are associated with a significant positive effect in *E. coli* in the antibiotic concentration it appeared during the DE experiment, yet the same mutation in the same antibiotic environment often did not confer a significant increase in fitness to the *K. pneumoniae* (Fig. 3a). Likewise, for the mutational steps selected in *K. pneumoniae* we see that they confer a significant fitness advantage to the mutant genotype over its immediate ancestor in the drug concentration where it was selected in the DE experiment (Fig. 3b). These mutations did not confer significant positive effects to *E. coli* in the same antibiotic concentrations, where the cost of the same resistance mutations did not sufficiently outweigh the level of drug inhibition for this more resistant species. This suggests the accessibility of plasmid mutations is determined both by the antibiotic environment but also the host genomic context.

Figure 3c-e show the relative fitness effect of plasmid mutations in *E. coli* (red) and *K. pneumoniae* (blue) that were selected in *E. coli* populations at concentrations marked by red triangles during the DE experiment. In panel c, we see the addition of a nucleotide substitution in the ribosome binding site (RBS) upstream of the gene is associated with a positive fitness effect

in staggered regions of concentration space between species. This RBS mutation likely affects protein expression and (along with substitution P22T in the periplasmic signal sequence)[48] requires the presence of M182T to significantly benefit either species. Figure 3d,e shows the mutation effect reaction norm for the E104A and E240K substitutions on the same triple mutant background. These mutations were selected in *E. coli* populations at 8 μg/mL where they both confer a large positive effect. In *K. pneumoniae*, the benefit of E104A is no longer realized while E240K remains slightly beneficial at this concentration.

We observe the converse shift in the analysis of selective accessibility for mutations selected in *K. pneumoniae* populations. The addition of A42G to the G238S background (Fig 3f) was sampled in both species during the DE experiment but with selection occurring in different antibiotic environments. In the barcoded fitness assay, we observe that this mutation is significantly beneficial to *K. pneumoniae* in lower concentrations compared to *E. coli*. Notably, we did observe a case of species-specific mutational effect with the addition of E104V to the H153R/G238S/T265M background, which conferred a significant positive effect to *K. pneumoniae* in 4 μg/mL where it was selected in the DE experiment (Fig 3g). This same step exhibited a substantial fitness cost to *E. coli* throughout most of the gradient, much larger than the typical fitness deficit of resistance mutations. Interestingly, *E. coli* could benefit from the addition of E104V to backgrounds if M182T (Fig 3h) is present instead of H153R. Incidentally, both species also benefit from the addition of E104K to either triple mutant background (Extended Data Fig. 3).

Discussion

This study combines directed evolution and bulk fitness assays to investigate how mutations in the plasmid-encoded *bla*$_{TEM}$ shape cefotaxime resistance across two bacterial host species, *E. coli* and *K. pneumoniae*. To our knowledge, this is the first DE experiment of TEM-1 with selection occurring in the *K. pneumoniae* host, which resulted in the selection of the D273E substitution alongside G238S in the first round. We note that this substitution has been observed in clinical surveillance of *bla*$_{TEM}$,[65] but not in previous directed evolution studies with this gene screening for resistance mutations in the *E. coli* host.[63] This highlights the importance of considering host background when searching for a comprehensive set of adaptive mutations in mobile genes.

Consistent with prior studies, we found that the identity of resistance-enhancing mutations often correlated between species.[24,35] However, we observed several cases of idiosyncratic fitness effects of the same mutation on the same genetic background in different host contexts. The most substantial species-specific effect was associated with the E104V substitution, which ironically was selected in both *E. coli* and *K. pneumoniae* during the DE experiment. In the barcoded fitness assay, we observed that E104V had an adaptive window in both species on the M182T/G238S/T265M background; however, the addition of E104V to H153R/G238S/T265M was beneficial in *K. pneumoniae* but highly costly in *E. coli*. Notably, H153R and T265M were more frequently selected in *K. pneumoniae* dyad members during the DE experiment while M182T was predominantly utilized in *E. coli*. All three substitutions conferred a fitness benefit when added to G238S in both species, but it is possible that subtle differences in compensatory effect size may have led to species-specific preferences in second-step mutations that later manifested as higher-order interactions with additional substitutions.

Through the adaptive window framework, our results demonstrate that mobile genes can follow divergent evolutionary paths within identical antibiotic environments depending on their host background. In this way, the landscape of accessible mutations is not only defined by selective pressures but also by the biological substrate on which those pressures act. While selective windows have often served as descriptive tools to explain resistance trajectories, we propose that they also represent structural features of a shifting evolutionary space, sensitive to deformations imposed by species-specific trade-offs in resistance and growth. This work lays the foundation for more general treatments of context-dependence in mobile gene evolution. In Chapter 2, we extend this framework by introducing a second host species to create mixed-species communities, enabling explicit tests of how ecological interactions reshape plasmid fitness and mutation accessibility across community contexts. As selection moves across increasingly complex landscapes, the rules of mutation, adaptation, and accessibility may themselves be rearranged — as if stepping through a looking-glass into a world where the same path leads to a different destination.

Bibliography

1. Ardell SM, Martsul A, Johnson MS, Kryazhimskiy S. Environment-independent distribution of mutational effects emerges from microscopic epistasis. Science. 2024 Oct 4;386(6717):87–92.

2. Artemova T, Gerardin Y, Dudley C, Vega NM, Gore J. Isolated cell behavior drives the evolution of antibiotic resistance. Mol Syst Biol. 2015 Jul;11(7):822.

3. Baquero F, Martínez JL, F. Lanza V, Rodríguez-Beltrán J, Galán JC, San Millán A, et al. Evolutionary Pathways and Trajectories in Antibiotic Resistance. Clin Microbiol Rev. 2021 Jun 30;34(4):e00050-19.

4. Cano AV, Gitschlag BL, Rozhoňová H, Stoltzfus A, McCandlish DM, Payne JL. Mutation bias and the predictability of evolution. Philos Trans R Soc B Biol Sci. 378(1877):20220055.

5. Cisneros-Mayoral S, Graña-Miraglia L, Pérez-Morales D, Peña-Miller R, Fuentes-Hernández A. Evolutionary History and Strength of Selection Determine the Rate of Antibiotic Resistance Adaptation. Mol Biol Evol. 2022 Sep 1;39(9):msac185.

6. Firnberg E, Labonte JW, Gray JJ, Ostermeier M. A Comprehensive, High-Resolution Map of a Gene's Fitness Landscape. Mol Biol Evol. 2014 Jun;31(6):1581–92.

7. Gillespie JH, Turelli M. Genotype-environment interactions and the maintenance of polygenic variation. Genetics. 1989 Jan;121(1):129–38.

8. Gupta A, Zaman L, Strobel HM, Gallie J, Burmeister AR, Kerr B, et al. Host-parasite coevolution promotes innovation through deformations in fitness landscapes. Ogbunugafor CB, Walczak AM, Barr J, editors. eLife. 2022 Jul 6;11:e76162.

9. Hietpas RT, Bank C, Jensen JD, Bolon DNA. Shifting fitness landscapes in response to altered environments. Evol Int J Org Evol. 2013 Dec;67(12):10.1111/evo.12207.

10. Johnson MS, Reddy G, Desai MM. Epistasis and evolution: recent advances and an outlook for prediction. BMC Biol. 2023 May 24;21(1):120.

11. Kryazhimskiy S, Rice DP, Jerison ER, Desai MM. Global Epistasis Makes Adaptation Predictable Despite Sequence-Level Stochasticity. Science. 2014 Jun 27;344(6191):1519–22.

12. Redondo-Salvo S, Fernández-López R, Ruiz R, Vielva L, de Toro M, Rocha EPC, et al. Pathways for horizontal gene transfer in bacteria revealed by a global map of their plasmids. Nat Commun. 2020 Jul 17;11(1):3602.

13. Salverda MLM, Koomen J, Koopmanschap B, Zwart MP, de Visser JAGM. Adaptive benefits from small mutation supplies in an antibiotic resistance enzyme. Proc Natl Acad Sci U S A. 2017 Nov 28;114(48):12773–8.

14. Sane M, Diwan GD, Bhat BA, Wahl LM, Agashe D. Shifts in mutation spectra enhance access to beneficial mutations. Proc Natl Acad Sci. 2023 May 30;120(22):e2207355120.

15. Schenk MF, Zwart MP, Hwang S, Ruelens P, Severing E, Krug J, et al. Population size mediates the contribution of high-rate and large-benefit mutations to parallel evolution. Nat Ecol Evol. 2022 Mar 3;6(4):439–47.

16. Yi X, Dean AM. Adaptive Landscapes in the Age of Synthetic Biology. Mol Biol Evol. 2019 May 1;36(5):890–907.

17. Trindade S, Sousa A, Xavier KB, Dionisio F, Ferreira MG, Gordo I. Positive Epistasis Drives the Acquisition of Multidrug Resistance. PLoS Genet. 2009 Jul 24;5(7):e1000578.

18. Bank C, Matuszewski S, Hietpas RT, Jensen JD. On the (un)predictability of a large intragenic fitness landscape. Proc Natl Acad Sci. 2016 Dec 6;113(49):14085–90.

19. Birgy A, Magnan M, Hobson CA, Figliuzzi M, Panigoni K, Codde C, et al. Local and Global Protein Interactions Contribute to Residue Entrenchment in Beta-Lactamase TEM-1. Antibiotics. 2022 May 13;11(5):652.

20. Phillips PC. Epistasis — the essential role of gene interactions in the structure and evolution of genetic systems. Nat Rev Genet. 2008 Nov;9(11):855–67.

21. MacLean RC, Perron GG, Gardner A. Diminishing Returns From Beneficial Mutations and Pervasive Epistasis Shape the Fitness Landscape for Rifampicin Resistance in *Pseudomonas aeruginosa*. Genetics. 2010 Dec 1;186(4):1345–54.

22. Weinreich DM, Delaney NF, DePristo MA, Hartl DL. Darwinian Evolution Can Follow Only Very Few Mutational Paths to Fitter Proteins. Science. 2006 Apr 7;312(5770):111–4.

23. Marciano DC, Karkouti OY, Palzkill T. A Fitness Cost Associated With the Antibiotic Resistance Enzyme SME-1 β-Lactamase. Genetics. 2007 Aug 1;176(4):2381–92.

24. Kosterlitz O, Grassi N, Werner B, McGee RS, Top EM, Kerr B. Evolutionary "Crowdsourcing": Alignment of Fitness Landscapes Allows for Cross-species Adaptation of a Horizontally Transferred Gene. Mol Biol Evol. 2023 Nov 3;40(11):msad237.

25. Salverda MLM, Dellus E, Gorter FA, Debets AJM, Oost J van der, Hoekstra RF, et al. Initial Mutations Direct Alternative Pathways of Protein Evolution. PLOS Genet. 2011 Mar 3;7(3):e1001321.

26. Weinreich DM, Knies JL. FISHER'S GEOMETRIC MODEL OF ADAPTATION MEETS THE FUNCTIONAL SYNTHESIS: DATA ON PAIRWISE EPISTASIS FOR FITNESS YIELDS INSIGHTS INTO THE SHAPE AND SIZE OF PHENOTYPE SPACE. Evolution. 2013 Oct;67(10):2957–72.

27. Weinreich DM, Lan Y, Wylie CS, Heckendorn RB. Should evolutionary geneticists worry about higher-order epistasis? Curr Opin Genet Dev. 2013 Dec;23(6):700–7.

28. Benz F, Hall AR. Host-specific plasmid evolution explains the variable spread of clinical antibiotic-resistance plasmids. Proc Natl Acad Sci. 2023 Apr 11;120(15):e2212147120.

29. Guerrero RF, Scarpino SV, Rodrigues JV, Hartl DL, Ogbunugafor CB. Proteostasis Environment Shapes Higher-Order Epistasis Operating on Antibiotic Resistance. Genetics. 2019 Jun 1;212(2):565–75.

30. San Millan A, Toll-Riera M, Qi Q, MacLean RC. Interactions between horizontally acquired genes create a fitness cost in Pseudomonas aeruginosa. Nat Commun. 2015 Apr 21;6(1):6845.

31. Dunn S, Carrilero L, Brockhurst M, McNally A. Limited and Strain-Specific Transcriptional and Growth Responses to Acquisition of a Multidrug Resistance Plasmid in Genetically Diverse Escherichia coli Lineages. mSystems. 2021 Apr 27;6(2):10.1128/msystems.00083-21.

32. Zheng J, Bratulic S, Lischer HEL, Wagner A. Mistranslation can promote the exploration of alternative evolutionary trajectories in enzyme evolution. J Evol Biol. 2021 Aug;34(8):1302–15.

33. Gama JA, Kloos J, Johnsen PJ, Samuelsen Ø. Host dependent maintenance of a blaNDM-1-encoding plasmid in clinical Escherichia coli isolates. Sci Rep. 2020 Jun 9;10(1):9332.

34. Jordt H, Stalder T, Kosterlitz O, Ponciano JM, Top EM, Kerr B. Coevolution of host–plasmid pairs facilitates the emergence of novel multidrug resistance. Nat Ecol Evol. 2020 Jun;4(6):863–9.

35. Knopp M, Andersson DI. Predictable Phenotypes of Antibiotic Resistance Mutations. mBio. 2018 May 15;9(3):10.1128/mbio.00770-18.

36. Lindsey HA, Gallie J, Taylor S, Kerr B. Evolutionary rescue from extinction is contingent on a lower rate of environmental change. Nature. 2013 Feb;494(7438):463–7.

37. Diaz-Colunga J, Sanchez A, Ogbunugafor CB. Environmental modulation of global epistasis in a drug resistance fitness landscape. Nat Commun. 2023 Dec 5;14:8055.

38. Ogbunugafor CB, Wylie CS, Diakite I, Weinreich DM, Hartl DL. Adaptive Landscape by Environment Interactions Dictate Evolutionary Dynamics in Models of Drug Resistance. PLoS Comput Biol. 2016 Jan 25;12(1):e1004710.

39. Mira PM, Meza JC, Nandipati A, Barlow M. Adaptive Landscapes of Resistance Genes Change as Antibiotic Concentrations Change. Mol Biol Evol. 2015 Oct;32(10):2707–15.

40. Steinberg B, Ostermeier M. Environmental changes bridge evolutionary valleys. Sci Adv. 2016 Jan;2(1):e1500921.

41. Schenk MF, Witte S, Salverda MLM, Koopmanschap B, Krug J, Visser JAGM. Role of pleiotropy during adaptation of TEM -1 β -lactamase to two novel antibiotics. Evol Appl. 2015 Mar;8(3):248–60.

42. Wortel MT, Agashe D, Bailey SF, Bank C, Bisschop K, Blankers T, et al. Towards evolutionary predictions: Current promises and challenges. Evol Appl. 2023 Jan;16(1):3–21.

43. Hall BG. Predicting Evolution by In Vitro Evolution Requires Determining Evolutionary Pathways. Antimicrob Agents Chemother. 2002 Sep;46(9):3035–8.

44. Barlow M, Hall BG. Predicting Evolutionary Potential: In Vitro Evolution Accurately Reproduces Natural Evolution of the TEM β-Lactamase. Genetics. 2002 Mar 1;160(3):823–32.

45. De Visser JAGM, Cooper TF, Elena SF. The causes of epistasis. Proc R Soc B Biol Sci. 2011 Dec 22;278(1725):3617–24.

46. Ogbunugafor CB. The mutation effect reaction norm (mu-rn) highlights environmentally dependent mutation effects and epistatic interactions. Evolution. 2022 Feb 1;76(s1):37–48.

47. Jacquier H, Birgy A, Le Nagard H, Mechulam Y, Schmitt E, Glodt J, et al. Capturing the mutational landscape of the beta-lactamase TEM-1. Proc Natl Acad Sci. 2013 Aug 6;110(32):13067–72.

48. Mehlhoff JD, Stearns FW, Rohm D, Wang B, Tsou EY, Dutta N, et al. Collateral fitness effects of mutations. Proc Natl Acad Sci. 2020 May 26;117(21):11597–607.

49. Mehlhoff JD, Ostermeier M. Genes Vary Greatly in Their Propensity for Collateral Fitness Effects of Mutations. Mol Biol Evol. 2023 Mar 1;40(3):msad038.

50. Mroczkowska JE, Barlow M. Fitness Trade-Offs in *bla* TEM Evolution. Antimicrob Agents Chemother. 2008 Jul;52(7):2340–5.

51. Reynolds MG. Compensatory evolution in rifampin-resistant Escherichia coli. Genetics. 2000 Dec;156(4):1471–81.

52. Gagneux S, Long CD, Small PM, Van T, Schoolnik GK, Bohannan BJM. The Competitive Cost of Antibiotic Resistance in Mycobacterium tuberculosis. Science. 2006 Jun 30;312(5782):1944–6.

53. Gullberg E, Cao S, Berg OG, Ilbäck C, Sandegren L, Hughes D, et al. Selection of Resistant Bacteria at Very Low Antibiotic Concentrations. Lipsitch M, editor. PLoS Pathog. 2011 Jul 21;7(7):e1002158.

54. Das SG, Direito SO, Waclaw B, Allen RJ, Krug J. Predictable properties of fitness landscapes induced by adaptational tradeoffs. eLife. 2020 May 19;9:e55155.

55. Farr AD, Pesce D, Das SG, Zwart MP, De Visser JAGM. The Fitness of Beta-Lactamase Mutants Depends Nonlinearly on Resistance Level at Sublethal Antibiotic Concentrations. Cooper VS, editor. mBio. 2023 Jun 27;14(3):e00098-23.

56. Stiffler MA, Hekstra DR, Ranganathan R. Evolvability as a Function of Purifying Selection in TEM-1 β-Lactamase. Cell. 2015 Feb;160(5):882–92.

57. Dasmeh P, Ton AT, Quach C, Serohijos AWR. Inferring the selection window in antimicrobial resistance using deep mutational scanning data and biophysics-based fitness models [Internet]. Evolutionary Biology; 2017 Sep [cited 2023 Jul 18]. Available from: http://biorxiv.org/lookup/doi/10.1101/189019

58. Ruelens P, de Visser JAGM. Choice of β-Lactam Resistance Pathway Depends Critically on Initial Antibiotic Concentration. Antimicrob Agents Chemother. 65(8):e00471-21.

59. Negri MC, Lipsitch M, Levin BR, Baquero F. Concentration-Dependent Selection of Small Phenotypic Differences in TEM ␣-Lactamase-Mediated Antibiotic Resistance. ANTIMICROB AGENTS CHEMOTHER. 2000;44.

60. Palzkill T. Structural and Mechanistic Basis for Extended-Spectrum Drug-Resistance Mutations in Altering the Specificity of TEM, CTX-M, and KPC β-lactamases. Front Mol Biosci. 2018 Feb 23;5:16.

61. Bradford PA. Extended-Spectrum β-Lactamases in the 21st Century: Characterization, Epidemiology, and Detection of This Important Resistance Threat. Clin Microbiol Rev. 2001 Oct;14(4):933–51.

62. Cantu C, Palzkill T. The Role of Residue 238 of TEM-1 β-Lactamase in the Hydrolysis of Extended-spectrum Antibiotics *. J Biol Chem. 1998 Oct 9;273(41):26603–9.

63. Salverda MLM, De Visser JAGM, Barlow M. Natural evolution of TEM-1 β-lactamase: experimental reconstruction and clinical relevance. FEMS Microbiol Rev. 2010 Nov 1;34(6):1015–36.

64. Sutcliffe JG. Nucleotide sequence of the ampicillin resistance gene of Escherichia coli plasmid pBR322. Proc Natl Acad Sci. 1978 Aug;75(8):3737–41.

65. Duarte IM, Amador P. In vitro transference and molecular characterization of blaTEM genes in bacteria isolated from Portuguese ready-to-eat foods. World J Microbiol Biotechnol [Internet]. 2011 Jan 1 [cited 2025 Mar 21]; Available from: https://www.academia.edu/20589921/In_vitro_transference_and_molecular_characterization_of_blaTEM_genes_in_bacteria_isolated_from_Portuguese_ready_to_eat_foods

Extended Data

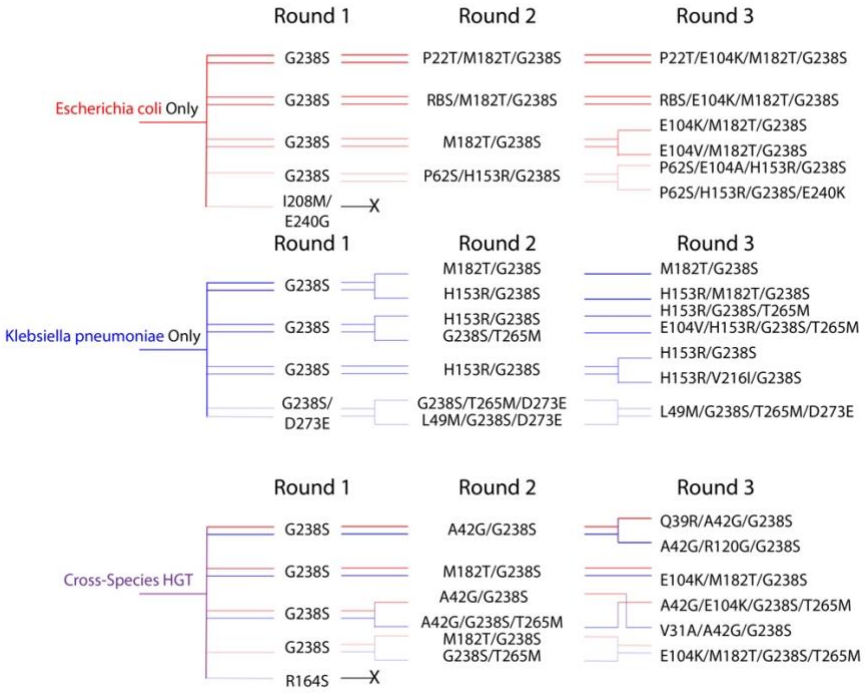

Extended Data Figure 1. Evolutionary trajectories taken throughout three rounds of directed evolution toward increased cefotaxime resistance. The four dyads comprising each treatment are indicated by shading and dyad members are colored by species (*E. coli* in red, *K. pneumoniae* in blue). Amino acid substitutions are reported as the residue that has been substituted, followed by the single letter designation for the mutant amino acid. RBS signifies a non-coding mutation in the ribosome binding site.

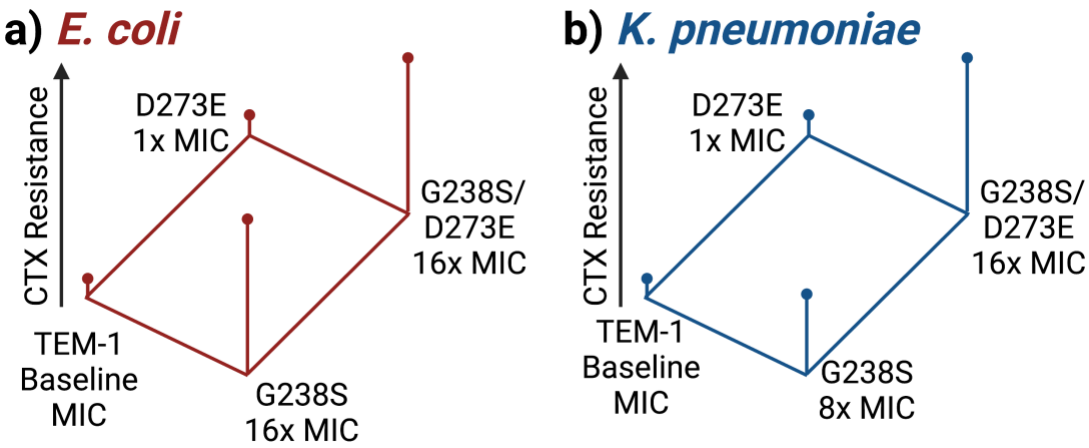

Extended Data Figure 2. Resistance landscapes of select genotypes as gauged by a traditional minimum inhibitory assay in both hosts. Note: Assay was conducted and gave identical results for 3 replicates of the plasmid selected in DE experiment and the reconstructed genotypes.

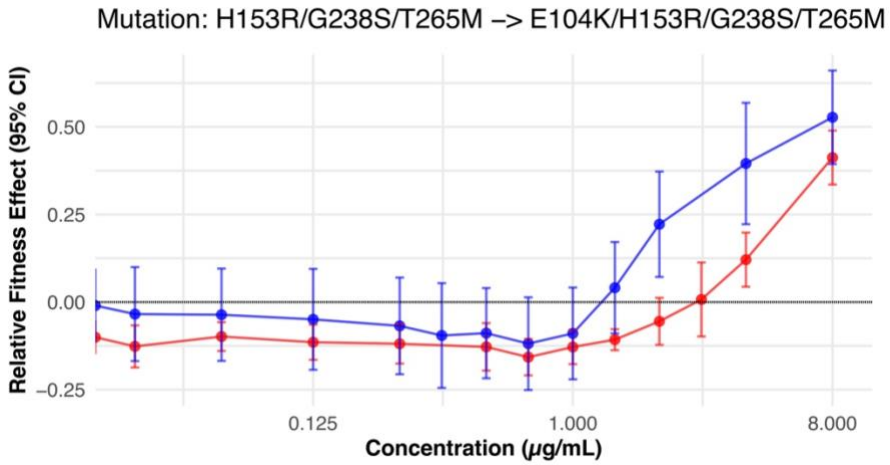

Extended Data Figure 3. Mutation effect reaction norm as a function of concentration for E104K substitution on the H153R/G238S/T265M background in both species.

Extended Methods

Directed Evolution Experiment

A culture of *Escherichia coli* grown overnight at 37 ˚C in LB + 15 µg/mL tetracycline to select for the presence of a modified pBR322 plasmid encoding $bla_{\text{TEM-1}}$. Following ~20 h of growth, a plasmid miniprep (Qiagen) was performed. This miniprep was divided among 12 independent error-prone polymerase chain reactions with Hot Start *Taq* Polymerase, a homemade mix of unbalanced deoxynucleotide triphosphates (200 µM ATP, GTP; 1 mM CTP, TTP) to combat mutational bias, primers compatible with Gibson Assembly that lie outside the *bla* coding DNA sequence, a 7 mM concentration of magnesium chloride cofactor, and ~0.5 µg of template plasmid. Amplification occurred in a BioRad thermocycler with a protocol of 95 ˚C for 3 minutes, followed by 30 cycles of 95 ˚C for 30 seconds, 50 ˚C for 30 seconds, 68 ˚C for 75 seconds, with a final extension at 68 ˚C for 5 minutes. PCR products were treated with DpnI at 37 ˚C for 30 minutes (followed by a heat inactivation step at 80 ˚C for 20 minutes) to selectively destroy methylated template plasmid and increase representation of mutant amplicons. Products were clean and concentrated using the Zymo Clean and Concentrator kit and eluted in 20 µL MilliQ water.

Vector backbones were prepared with high-fidelity amplification by Q5 DNA polymerase followed by DpnI digestion to remove methylated template plasmid. Separate barcodes were used to track evolutionary lineages each round to detect line swaps. Mutagenized insert and faithfully amplified vector fragments were combined using Gibson Assembly with 50-100 ng of vector and insert at a 2- or 3-fold molecular excess. Ligated product was transformed into chemically competent E. coli and cultures were miniprepped following ~20 h growth. Next, 4 µL of plasmid miniprep was electroporated into homemade aliquots of electrocompetent *E. coli* and *K. pneumoniae*. Note: the additional growth phase in *E. coli* was implemented because of the low transformation efficiency of *K. pneumoniae*, which improved when using methylated miniprep plasmid as compared to Gibson product. Libraries sizes each round were at least 10^5 for *K. pneumoniae* and 10^6 for *E. coli*.

The 12 error-prone polymerase chain reactions represent the 12 evolution lines each of which was transformed into two dyad members. Four pairs of these dyad members comprised three distinct treatments, with two replicates of the same species in the *E. coli* only and *K. pneumoniae* only treatments and one population of each species in the cross-species HGT

treatment. Following separate transformations for the 24 dyad members, transformant library size was estimated via selective plating on LB + 15 µg/mL tetracycline and used to inoculate separate LB cultures with a final concentration of 15 µg/mL. After ~20 h of growth, each culture was pelleted at 4750 rpm for 10 min in a Beckman-Coulter tabletop centrifuge, the supernatant was decanted, and the pellet was resuspended in equal volumes of fresh Mueller-Hinton broth.

This washed culture was then diluted 1:1000 to form a culture twice as dense as the initial inoculum. Plating was used to estimate density from this culture then 2.5 mL of culture was mixed with 2.5 mL of drug media. The gradient was prepared by dissolving 50 mg of cefotaxime powder (Sigma) in 10 mL MilliQ water to prepare a 5 mg/mL stock that was filter sterilized and distributed into 1 mL aliquots and stored at -20 ˚C. On the day of the assay, an aliquot was thawed and mixed with MH broth to form a gradient of 2x working concentrations, of which 2.5 mL was transferred to test tubes to be diluted 1:2 by bacterial culture in 18 mm test tubes. The MIC tubes were incubated at 37 ˚C with shaking for ~20 h then the culture for each dyad member at the highest concentration to reach visible turbidity was diluted $1{:}10^6$ and plated onto LB + 15 µg/mL tetracycline plates. The next day, a single colony was randomly selected to initiate a LB + 15 µg/mL tetracycline culture which was subjected to a plasmid miniprep (Qiagen) after ~20 h of growth. Plasmids from each dyad member were Sanger sequenced (Azenta) to identify the selected mutation(s).

Prior to the second round, the insert region of the plasmid was first amplified using Q5 DNA polymerase in a high-fidelity PCR. This enabled careful quantification of the gene fragment between species as to not overweight the contribution of one species due to copy number differences. These products were treated with DpnI to selectively remove template DNA as described then processed using the Zymo Clean and Concentrator kit and eluted in 20 µL of MilliQ water. To enable sharing of genotypes and immediate mutational neighbors, plasmids were mixed in equal amounts between dyad members belonging to the same evolution line. These 12 plasmid mixtures were added to the second round of error-prone PCR to acquire ~120 ng of DNA template adjusting the volume of water but keeping the concentrations of *Taq* DNA polymerase, $MgCl_2$, and dNTPs identical to the previous round. This mutagenized fragment was ligated into uniquely barcoded vectors using Gibson Assembly as before. Transformations and selection occurred as it did in the first round but with each dyad member inoculated across a gradient with beginning at the MIC of the previous round. The third round was performed in an identical fashion to the second. Sanger sequencing results at each round revealed synonymous and nonsynonymous changes in the coding DNA sequence. To restrict the number of genotypes to engineer, we chose to reconstruct only nonsynonymous changes for analysis.

Genetic Engineering

All directed evolution genotypes were constructed using the Q5 site-directed mutagenesis kit with homemade aliquots of *E. coli* K12 (DH10B). In short, polymerase chain reaction with a high-fidelity DNA polymerase (Q5) were performed with two "back-to-back" primers with the forward primer encoding the same nucleotide changes sampled during the DE experiment. PCR products were treated with the NEB Kinase, Ligase, and DpnI (KLD) kit. This kit facilitates the recircularization of the linear PCR product by phosphorylating (kinase) then fusing (ligase) the ends of the newly synthesized DNA molecule. KLD products will be transformed into homemade, chemically competent *E. coli* then Sanger sequenced (Azenta Biosciences) to ensure proper construction. Following confirmation, individual colonies with properly constructed

alleles were used to initiate LB + 15 µg/mL cefotaxime cultures, grown overnight, then the plasmid was isolated using a Qiagen miniprep kit.

These plasmid minipreps were double-digested with NcoI-HF and NsiI-HF restriction endonucleases and treated with recombinant shrimp alkaline phosphatase to prevent recircularization of the vector. Separately, a barcoded insert molecule was constructed using a ~200 bp primer of which the interior contains a stretch of 18 unspecified (NNN) nucleotides. These single-stranded primers were filled in with the Klenow (exo-) fragment, then these insert oligonucleotides were digested with NcoI-HF and NsiI-HF and ligated into the linear vector using the T4 ligase enzyme. Ligated product was transformed into 100 µL aliquots of homemade chemically competent *E. coli.* Barcode sequences for all isolates were identified via Sanger sequencing and the full gene plus barcode region was sequenced for one replicate per genotype.

Barcoded Monoculture MIC Experiment

Library Preparation

The mutational steps comprising the trajectories from TEM-1 to the 18 unique high resistance genotypes acquired as endpoints from three rounds of directed evolution toward increased CTX resistance were reconstructed. These genotypes were barcoded in triplicate and one barcoded replicate of these additional genotypes were added to three separate plasmid libraries: Lib I, II, III. Plasmid libraries were processed using the Zymo Clean and Concentrator Kit then individually transformed into three 100 µL aliquots of homemade electrocompetent cells of *E. coli* and *K. pneumoniae* using a Gene Pulser apparatus with a field strength of 2.5 kV and a time constant of ~6 ms. Competent cells were resuspended in 950 µL LB, transferred to 1.7 mL microcentrifuge tubes (Eppendorf), and recovered at 37 ˚C with shaking for 1 hour. Transformant library size was estimated via plating on LB agar + 15 µg/mL tetracycline and 800 µL of the library was used to inoculate six (Lib I, II, III in *E. coli* and *K. pneumoniae*) LB + 15 µg/mL tetracycline (final concentration) cultures grown overnight.

Following a growth phase of ~20 h, 4 mL of saturated transformant cultures were separately spun down in 15 mL centrifuge tubes at 4750 rpm for 10 min. The supernatant was decanted, and *E. coli* cell pellets were resuspended in 4 mL and *K. pneumoniae* cell pellets were resuspended in 6 mL to adjust for species-specific differences in yield. Equal volumes (2 mL) of Lib I, II, III were mixed between *E. coli* and *K. pneumoniae* to form monocultures containing three barcoded replicates for each genotype. These mixed cultures were diluted 1:1000 (200 µL culture in 200 mL MH broth) then 2.5 mL of diluted culture was mixed with 2.5 mL of drug media in 18 mm test tubes during the barcoded MIC experiment. The inoculum density for *E. coli* was $5.2 * 10^5$ CFU/mL and *K. pneumoniae* was $7.9 * 10^5$ CFU/mL based on plating from the 1:1000 culture adjusted for the 1:2 dilution into the gradient. Densities of both species at all timepoints were collected from LB + 15 µg/mL tetracycline plates.

Gradient Preparation

To prepare the antibiotic gradient, 410 mg cefotaxime powder (Sigma) was added to 10 mL molecular grade sterile distilled water (Invitrogen) to form a 41 mg/mL stock solution, which is ~40x the working concentration of the highest concentration tested (1024 µg/mL). The 41 mg/mL stock solution underwent serial 1:2 dilutions (5 mL stock in 5 mL of water) to form a 40x working concentration gradient ranging from 1024 µg/mL to 0.015 µg/mL that was stored at -80 ˚C. A1 mL aliquot of each concentration in the 40x working concentration was removed from the freezer on the day of the assay and thawed. 900 µL of each CTX concentration was mixed with

17.1 mL MH broth in separate 50 mL centrifuge tubes. This 1:20 dilution yielded a 2x gradient that is diluted to the appropriate test concentration when combined with 2.5 mL of diluted culture. Additionally, 8.49 mL of certain log2 concentrations were mixed with 3.51 mL MH broth to form the adjacent log SQRT (2) cefotaxime concentration for increased resolution in the middle of the gradient. Both species were inoculated across the following cefotaxime concentrations: 0, 0.03, 0.06, 0.125, 0.25, 0.35, 0.5, 0.7, 1, 1.4, 2, 2.8, 4, 5.7, 8, 11.3, 16, 22.6, 32, 45.3, 64, 128, 256 µg/mL but only select samples were sequenced to obtain barcode information.

Experimental Assay

After inoculation of the two species gradients, test tubes were incubated at 37 ˚C with shaking. Cultures were removed from the incubator at 3.5 h, 1 mL was removed from every culture, transferred to a 1.7 mL microcentrifuge tube, and stored on ice to preclude growth. A portion of this aliquot was used in a dilution series to estimate culture density while the remaining volume was pelleted at 13,000 rpm for 10 min in a microcentrifuge (Eppendorf), the supernatant was decanted, and the wet cell pellet was stored at -20 ˚C for subsequent amplification of the barcode region. Cultures were similarly sampled at t = 5 and t = 20 but the analysis for this study will be restricted to the 3.5 h timepoint to describe the short-term competitive dynamics before drug degradation and social effects compound.

Fitness Analysis

Plasmid genotype frequencies were estimated by proxy through short-read amplicon sequencing of the associated barcode region. Cell pellets were thawed from -20 ˚C and 1 µL of this cell suspension was used as template in a culture PCR with Q5 DNA polymerase and primers bearing partial Illumina adapters. Each experimental sample was individually amplified, cleaned, normalized to 20 ng/µL, and submitted for EZ amplicon sequencing by Azenta Biosciences. Barcode-level growth rates were calculated as:

$$r_{i,c,s} = \frac{1}{3.5}\left\{\ln \frac{f_{i,c,s}(3.5)D_{c,s}(3.5)}{f_{i,c,s}(0)D_{c,s}(0)}\right\}$$

where $f_{i,c,s}(t)$ denotes the frequency of the i^{th} barcode in media with a drug concentration of c in species s at time t and $D_{c,s}(t)$ is the total culture density of species s in media with a drug concentration of c at time t . Genotypic growth rates were computed as the mean of all barcoded replicates within the same antibiotic concentration and species (i.e., averaging $r_{i,c,s}$ over the relevant i values while fixing c and s). More technically, suppose the set of barcodes corresponding to genotype g is given as $\mathbf{B}_g$, then we have the mean growth rate of this genotype

$$\bar{r}_{g,c,s} = \frac{1}{|\mathbf{B}_g|}\sum_{i\in\mathbf{B}_g} r_{i,c,s}$$

To represent statistical uncertainty around plasmid genotype fitness estimates, 95% confidence intervals (CIs) were computed for each genotype across antibiotic concentrations and species.

For each genotype (g), drug concentration (c), and species (s), the standard error of the mean growth rate was calculated from the set of barcode replicates

$$SE_{g,c,s} = \frac{SD([r(i,c,s): i \in \mathbf{B}_g}{\sqrt{|\mathbf{B}_g|}}$$

where SD denotes the standard deviation of barcode-level growth rates. The 95% confidence interval around the mean growth rate was then defined as:

$\text{CI95\%} = \bar{r}_{g,c,s} \pm 1.96 \times SE_{g,c,s}$

These intervals were used to determine the statistical significance of fitness effects within each species. A mutational step was considered statistically significant within a species if the 95% CI for the fitness difference between mutant neighbors did not overlap with zero. Two independently prepared and sequenced $t = 0$ samples for each species were used to confirm consistency in the initial distribution of genotypes prior to selection across the cefotaxime gradient. Following a log10 transformation, initial barcode frequencies exhibited high concordance between replicates in both species (Pearson correlation coefficient 0.96 in *E. coli* and 0.91 in *K. pneumoniae*).

Edges in Figure 3 represent the relative fitness effect of each mutation at a single antibiotic concentration: the Maximum Growth Concentration (MGC) where the mutant genotype was selected in the directed evolution experiment (Figure 1). If a mutant genotype appeared at multiple MGCs, the most frequently observed concentration was used; in the case of ties, the lowest MGC was selected. Double mutants selected in the DE experiment were reconstructed and evaluated as individual mutational steps at the MGC of the double mutant.

Edges represent the scaled fitness effect of each mutation in the antibiotic concentration that it was selected in *E. coli* (Fig 3a) or *K. pneumoniae* (Fig 3b). To account for host-specific differences in baseline growth, we implement a mutant-weighted scaling factor that gives greater weight to mutations with higher absolute fitness. This approach is particularly relevant in our plasmid-based system, where differences in host growth rate (e.g., faster baseline growth in *Klebsiella pneumoniae*) can inflate raw fitness values without proportionally increasing the selective advantage of plasmid mutations. All network plots and growth rate analyses were implemented in R using the tidyverse, ggplot2, and igraph packages.

Chapter 2
Host and Habitat: Ecological Context Shapes Evolution of a Mobile Gene

Nathan Grassi, Fischer Tsai, Benjamin Kerr

Abstract

Mobile genetic elements such as plasmids experience selection across diverse host species, rendering their evolutionary fate partially decoupled from that of any single genome. Here, we quantify how host community composition modulates the selective accessibility of resistance mutations in the mobile *bla*TEM gene. Using barcoded libraries of 39 plasmid genotypes in *Escherichia coli* and *Klebsiella pneumoniae*, we measure genotypic fitness and mutation effects across a cefotaxime gradient in both monoculture and coculture. We find that coculture deforms plasmid fitness landscapes in species-specific ways, structured by baseline trade-offs in resistance and growth. These deformations shift the relative accessibility of mutations, with some resistance-enhancing genotypes benefiting from interspecies interactions, specifically reduced environmental drug pressure due to enzymatic detoxification. Thus, we show that plasmid adaptation emerges from coupled eco-evolutionary dynamics, where selection within host species is entangled with community-level interactions. This finding highlights the need to account for host community structure when predicting the evolutionary trajectories of mobile genetic elements under antibiotic selection.

Introduction

Mutational effects are fundamentally contextual, and the fitness conferred by a genetic change depends not only on the physical environment but also on the genetic and ecological conditions in which it arises.[1–7] Recent work has emphasized the conceptual overlap between genetic epistasis and ecological interactions, suggesting that both can be described within a shared framework of context-dependent fitness effects.[8–22] Mapping the modulation of fitness effects between mutationally-adjacent genotypes through perturbations to multiple ecological factors can provide insight into general principles of context-driven adaptation.[9–13,15,18,19,21,23–40] Mobile genetic elements offer a unique perspective into this complexity due to their evolutionary fate not being necessarily tied to the fitness of a single genome.[41–47]

Instead, plasmid-encoded genes experience selection across multiple host backgrounds, each with its own physiological constraints and ecological dynamics.[41,43,44,47–49] Thus, mobile elements are coupled evolving entities—linked to their hosts like mutualistic partners, yet subject to independent selective pressures.[48,49] Mutations in plasmid-encoded genes interact with the chromosomal background of the host, the physical environment (e.g., antibiotic concentration), and the broader microbial community.[44,46–51] In the case of enzyme-mediated resistance (e.g., beta-lactamases), the environment itself is dynamic as hydrolysis causes the antibiotic concentration to decline over time.[25,52–56] This means that genotypes interact not only with their surroundings but also with the consequences of their collective enzymatic activity.[53–56] This creates opportunities for social interactions in competitions between genotypes within a host species and between host–plasmid pairings in multispecies communities.[15,53,55,55–57]

This work builds on our previous study to understand how the evolution of mobile genes is affected by host background and horizontal gene transfer.[58] Previously, we demonstrated mutations in plasmid-encoded *bla*TEM that increase cefotaxime resistance phenotype in one host often retain similar effects in others, enabling species to crowdsource resistance evolution. Next, we selected for mutational trajectories toward cefotaxime resistance in *E. coli* and *K. pneumoniae* host backgrounds in a directed evolution experiment then performed bulk fitness

assays in monoculture (Grassi, et al Chapter 1). We found that acquisition of CTX resistance mutations elicits a classic trade-off in both species where mutations that confer higher resistance often reduce growth rate in low-drug environments. Moreover, due to differences in baseline resistance and physiological cost structures, the region of concentration space where these costly resistance mutations confer a benefit (i.e., the adaptive window) differed between species.

In the present study, we compare genotypic fitness and mutational fitness effects across host community structures including species monocultures and coculture. We show that the introduction of a second host species reshapes the adaptive windows of plasmid mutations. These context-dependent deformations reflect the species-specific trade-offs in competitive ability and resistance observed in monocultures, which furthermore parallel the constraints observed between genotypes within a single species. The evolutionary accessibility of plasmid mutations thus hinges upon numerous factors within the potentially shifting ecological setting, underscoring the importance of incorporating host background and host community structure to predict the evolutionary potential of mobile genetic elements.

Results

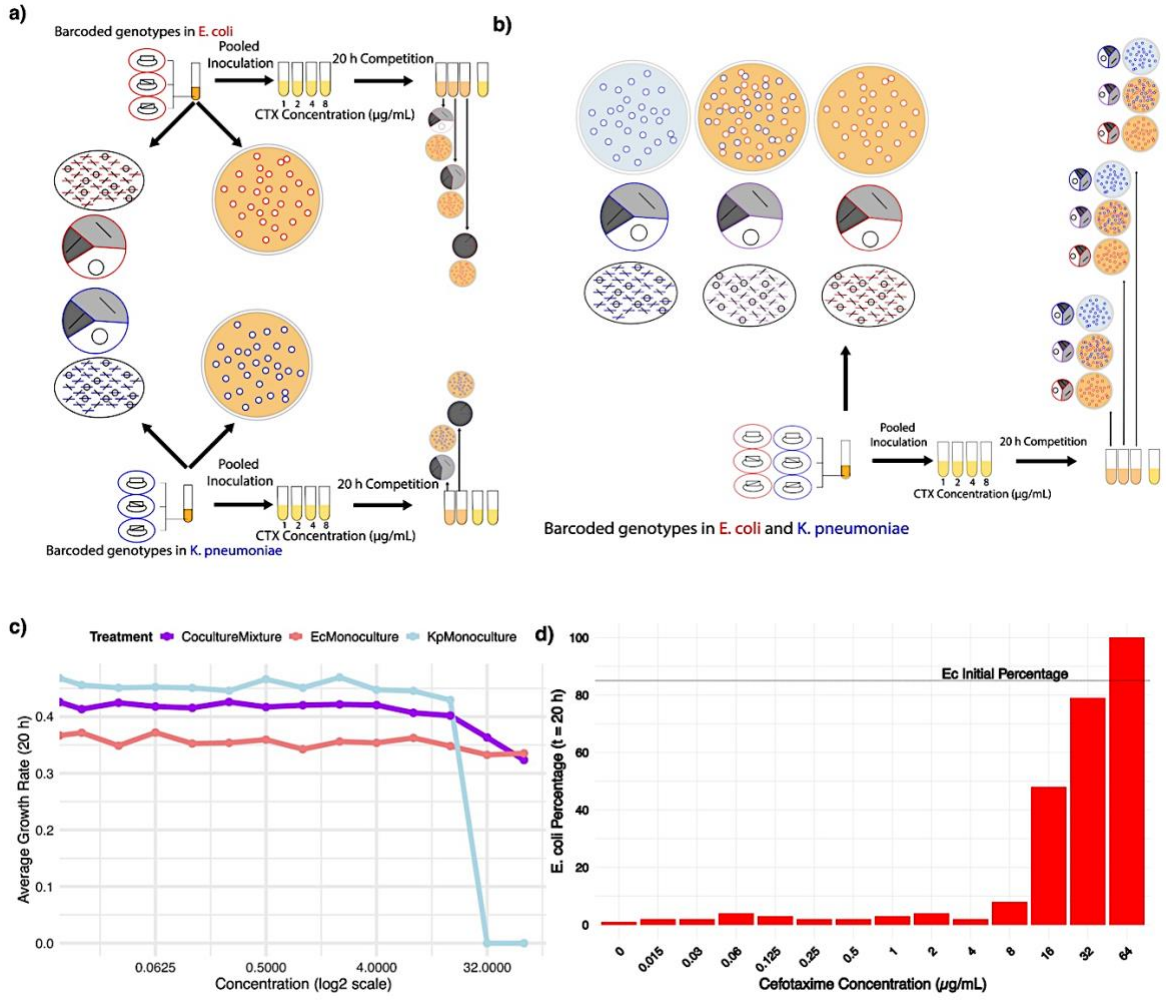

Figure 1. a) Schematic of bulk fitness assays in monocultures of *E. coli* and *K. pneumoniae*. A library of 39 plasmid genotypes each with three replicate barcode sequences downstream of the bla_{TEM} coding DNA sequence were introduced into each species and competed across a 2-fold gradient of cefotaxime. Barcode densities (the product of barcode frequency and total culture density) were tracked over 20 hours in each competition environment to calculate plasmid genotypic fitness. b) Schematic of coculture bulk fitness assay. The three barcoded replicates

comprising each plasmid genotype were distributed between species so that one barcode sequence per genotype appeared in *E. coli* only, one in *K. pneumoniae* only, and one in both (hybrid). Plasmid fitness was estimated using barcode frequency multiplied by total culture density. Separately, selective plating for chromosomal resistance markers in each species was used to estimate host community composition of each population c) Average growth rate over 20 h is reported for the three tested host populations (*E. coli* monoculture, red; *K. pneumoniae* monoculture, blue; Coculture, purple) as a function of antibiotic concentration. d) Percentage of *E. coli* in coculture environments following 20 h of competition. The dashed line represents the initial proportion of *E. coli* (85% of 5.8 x 10^5 CFU/mL) in the shared inoculum of each environment. *E. coli* percentage was calculated based on densities derived via selective plating [*E. coli* density / (*E. coli* density + *K. pneumoniae* density)].

Here, we measure plasmid genotypic fitness across a cefotaxime (CTX) gradient in monoculture and coculture competitions involving *E. coli* and *K. pneumoniae* (Fig. 1a-b). Competition of plasmid genotypes within these three host communities occurred on the same day with the same antibiotic gradient. Fitness was calculated for each barcode in all three communities as the log change in barcode density (barcode frequency * total culture density) over the 20 h competition. Total culture density was assessed by selective plating on tetracycline-laced plates for a plasmid-encoded resistance marker (*tetA*) expressed in both host species. In monoculture, each genotype is tracked by three unique barcode sequences in each species. These barcodes are distributed in coculture so that one barcode-genotype combination appeared in *E. coli* only, one in *K. pneumoniae* only, and one in both species.

Over 20 hours of growth, *K. pneumoniae* monocultures consistently reached ~3-fold higher cell yields than *E. coli*, a trend reflected in elevated genotypic fitness values in most tested antibiotic environments (Fig. 1b). Since final barcode density is derived by multiplying barcode frequency by final culture density, the higher yield of *K. pneumoniae* contribute to an overall upward shift in fitness values. The pooled genotypic library in *K. pneumoniae* achieves a higher yield in 0-16 µg/mL CTX but does not form a turbid culture in 32 or 64 µg/mL CTX where *E. coli* does (Fig. 1c). In addition, our prior observations from short-term competitions (3.5 h) indicate that *K. pneumoniae* has a faster maximal growth rate, but reduced resistance compared to *E. coli* (Grassi et al., Chapter 1).

The superior competitive ability of *K. pneumoniae* caused the final composition of populations in all but the highest drug pressure to heavily favor this species (Fig. 1d). Estimates of community composition from species-specific selective plating indicate that *K. pneumoniae* comprises >90% of cocultures in the low to intermediate drug environments (0-8 µg/mL). In 16 µg/mL, which is the maximum concentration for which *K. pneumoniae* monoculture exhibits turbid growth over 20 h, *E. coli* comprises 48% of the coculture population. In 32 µg/mL, *E. coli* constitutes close to its initial proportion (79% final; 85% initial), while in 64 µg/mL, *K. pneumoniae* was not detectable by species-specific plating. The genotypes and species share antibiotic environments in the bulk fitness assays, which due to the nature of beta-lactamase mediated resistance is a dynamic environment where drug concentration decreases over time. Genotypes or species with more functional enzyme can detoxify the environment and permit survival of less resistant, but potentially more competitive, types. Although *K. pneumoniae* monoculture failed to yield a turbid culture at 32 µg/mL, *K. pneumoniae* in coculture benefitted from the presence of *E. coli* and achieved a high density (1.6 x 10^8 CFU/mL) in coculture, a case of interspecific social protection.

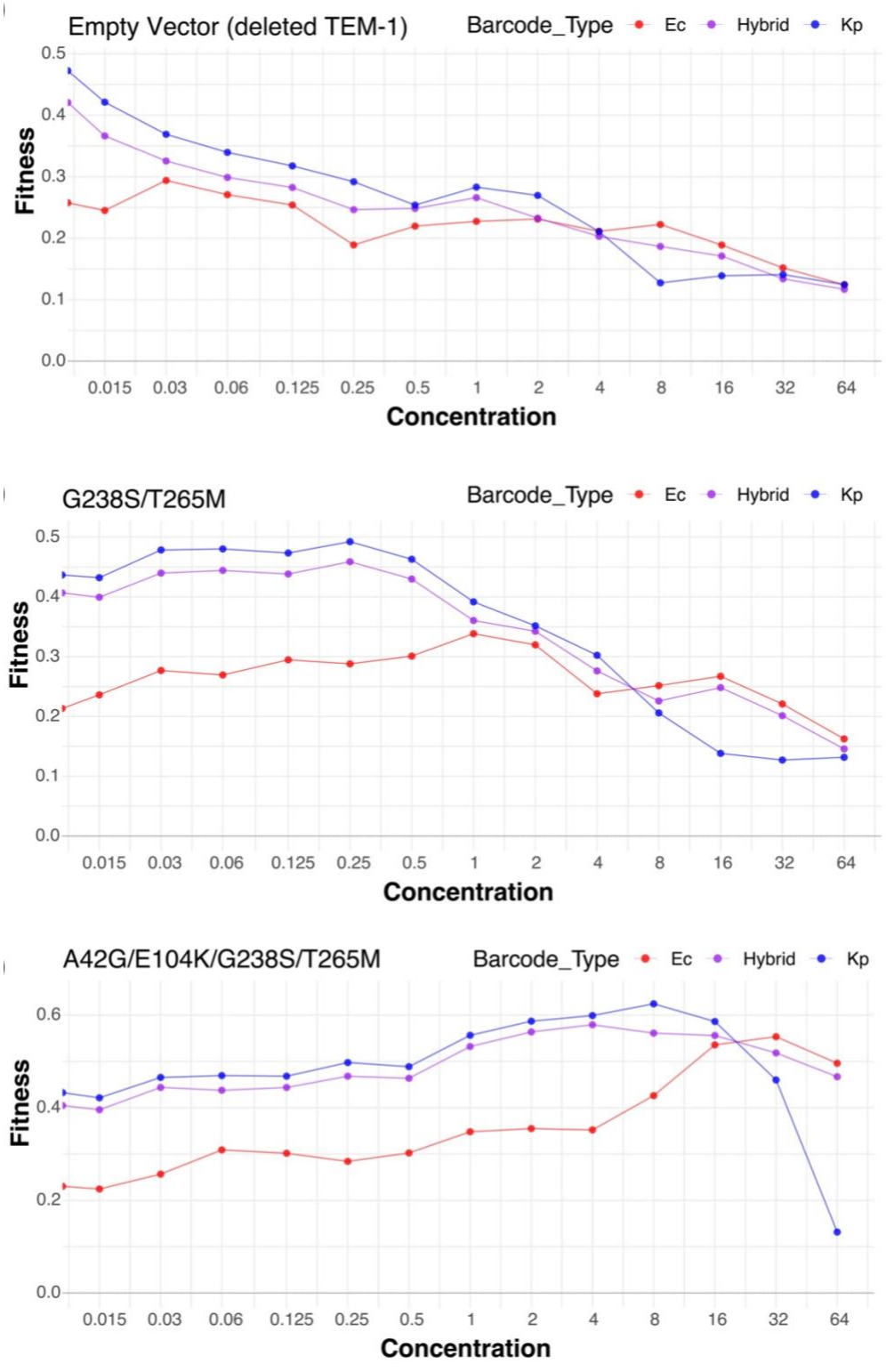

Figure 2. The 20 h growth rate in coculture competitions of three replicate barcode plasmids encoding the same genotype (deleted bla_{TEM} gene in a, G238S/T265M in b, A42G/E104K/G238S/T265M in c) hosted by *E. coli* (red), *K. pneumoniae* (blue), or both species (purple) plotted as a function of cefotaxime concentration.

Due to differences in host fitness, plasmid genotypes harbored by *K. pneumoniae* consistently outcompete the same genotype hosted by *E. coli* or both species in most concentrations evaluated in the coculture assay (Fig. 2). However, plasmid genotypes repeatedly exhibit higher fitness in *E. coli* under increased drug pressure, but where this crossover occurs depends on the resistance capacity of the genotype. In Fig. 2a, we compare plasmid fitness of an empty vector control, which retains the plasmid-encoded tetracycline resistance marker but from which the bla_{TEM} is deleted. This genotype possesses a high baseline growth rate but a low resistance capacity relative to other genotypes within the same species. The G238S/T265M genotype, contains two substitutions which in combination increase resistance in both species (Grassi et al, Chapter 1). This enhanced resistance allows this genotype to exhibit a higher net growth rate in intermediate drug concentrations over 20 h within both species as compared to the empty vector. Moreover, the enhanced resistance of the double mutant shifts the intersection where *E. coli* becomes the more fit host higher in concentration space compared to the less resistant genotype (Fig. 2b).

The fitness of the high resistance genotype, A42G/E104K/G238S/T265M, within each species reaches its maximum value in higher drug concentrations where fewer variants survive over the course of 20 h. In other words, the most resistant types benefit from a reduction in the number of surviving competitors as antibiotic concentration increases. Again, we observe this pattern in comparisons of different plasmid genotypes competing within the same species or between the same plasmid genotype competing between different species. In coculture at 32 µg/mL, *E. coli* is the more fit host of this plasmid genotype, but this genotype still possesses a large positive fitness in *K. pneumoniae* at this concentration. Importantly, the 32 µg/mL is the only antibiotic concentration where coculture exhibits a higher final density than either monoculture (Fig. 1c), suggesting that interspecies cooperation enables some high resistance genotypes in *K. pneumoniae* to be salvaged by *E. coli* in coculture. At 64 µg/mL, the coculture final density (Fig. 1c) and species proportions (Fig. 1d) resemble an *E. coli* monoculture where even the most resistant genotypes in *K. pneumoniae* are substantially inhibited by drug (Fig 2c).

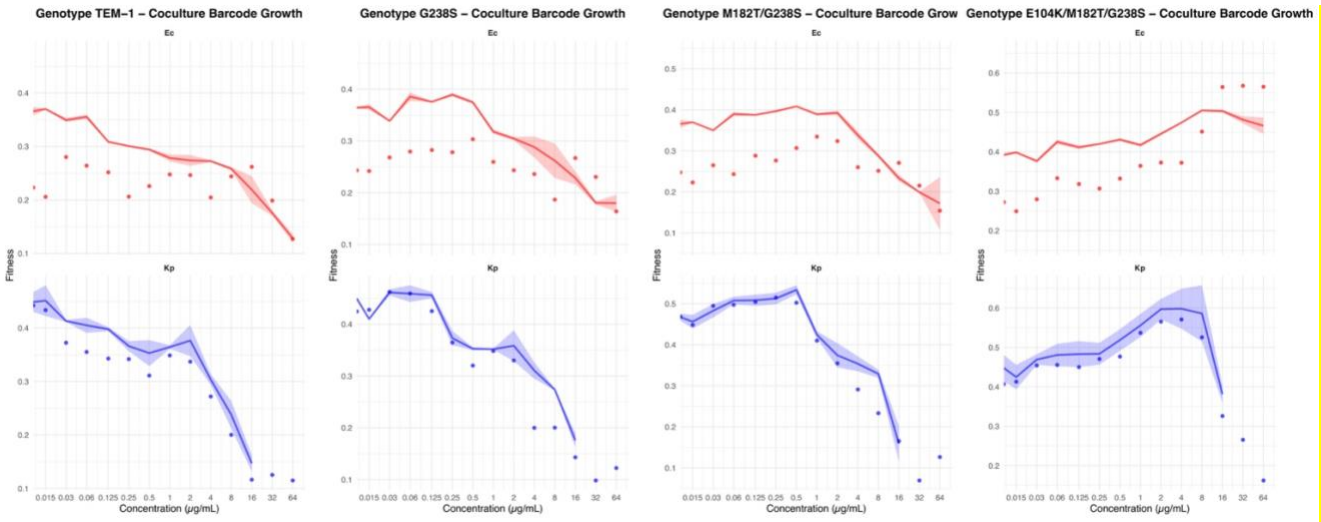

Figure 3. a-d) Individual data points represent fitness of barcoded plasmid genotypes from prior directed evolution experiment in coculture environment hosted exclusively by *E. coli* (Ec, red) or *K. pneumoniae* (Kp, blue); hybrid barcode data not shown. Connected points represents mean genotypic fitness in *E. coli* or *K. pneumoniae* monoculture (shading represents 95% CI).

We next compare plasmid genotype fitness in each host species in coculture compared to each species monoculture. The genotypes included in Fig. 3 represent a mutational trajectory to a high resistance genotypic endpoint sampled by both species in a prior DE experiment (Grassi et al, Chapter 1). Moreover, this genotypic endpoint is frequently encountered in both clinical and laboratory evolution of TEM-1 to increased cefotaxime resistance.[62] Fitness of these genotypes hosted by *E. coli* in coculture were consistently lower than genotypic fitness in monoculture throughout low to intermediate drug concentrations (Figure 3). Fitness of *K. pneumoniae* genotypes were more similar between host communities throughout these concentrations, consistent with the competitive dominance of this species in these environments.

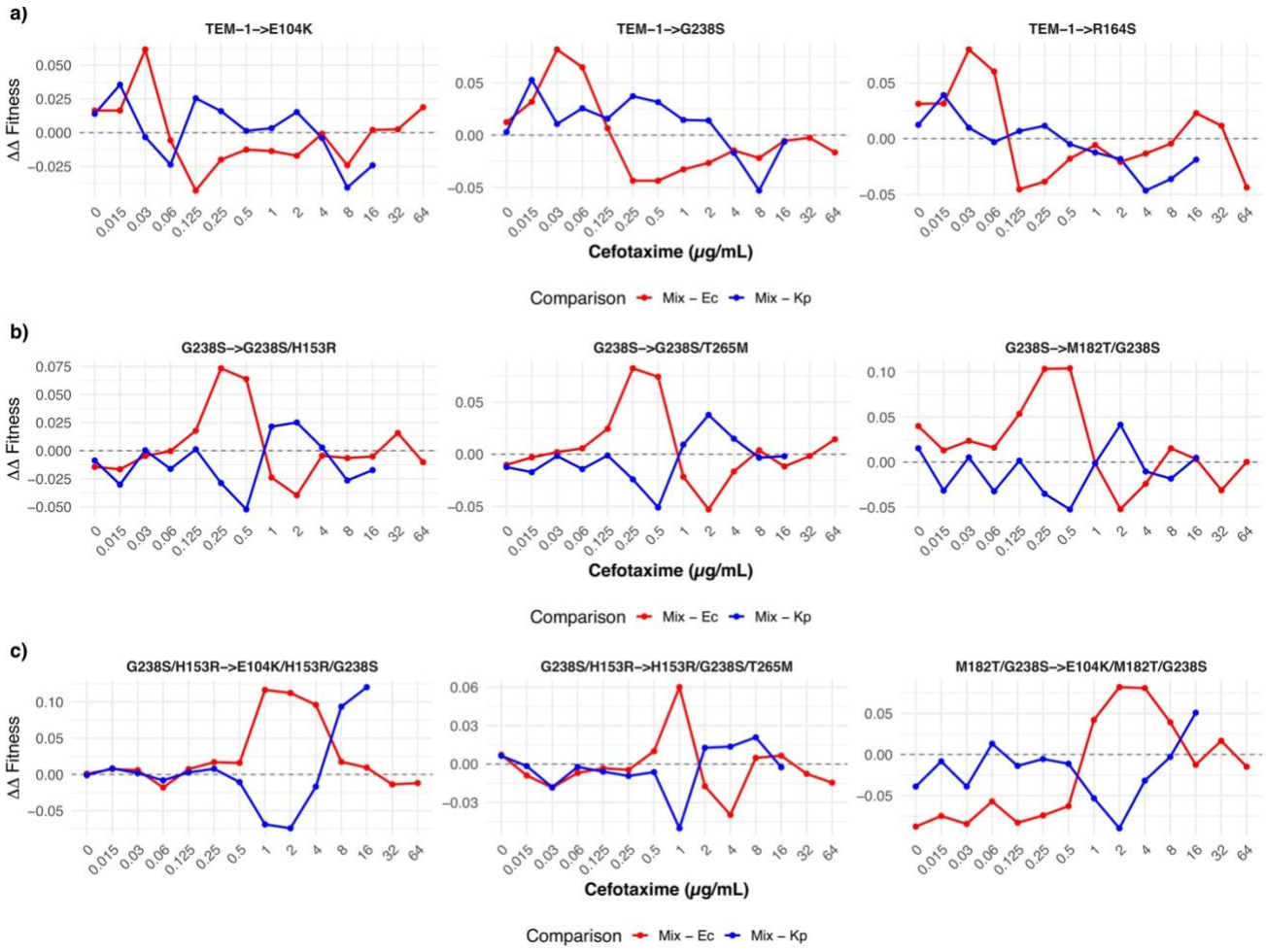

Figure 4. Population-level deformation of mutational effect across ecological contexts. Each plot shows the difference in relative fitness effect for a resistance-enhancing mutation across the antibiotic gradient. As in Chapter 1, we calculate the relative fitness difference of mutant neighbor genotypes to estimate mutational effect. Fitness differences between genotypes are performed within barcode type, comparing fitness of mutationally adjacent alleles within the same species in coculture or within pseudo-replicates in monoculture. These differences are averaged to estimate a population-level fitness effect within each environment and host community. Next, we plot the difference in mutational effect between coculture "Mix" – *E. coli* monoculture in red and coculture "Mix" – *K. pneumoniae* monoculture in blue for resistance mutations in genetic backgrounds with no (a), one (b), or two (c) existing mutations. Positive values indicate that the mutation was associated with a more positive effect in coculture than in the respective monoculture; negative values indicate that the mutation was less beneficial in coculture.

To interrogate the impact of community structure on plasmid evolution we calculate the difference in mutational effect in coculture compared to each monoculture (Figure 4). This difference reflects how the fitness effect of resistance mutations in identical antibiotic environments shifts between monoculture and coculture communities. Within the coculture "Mix" treatment, fitness differences between mutant neighbor genotypes in each drug environment are calculated within host barcode type so that plasmid mutational effect is inferred within each species background. These fitness differences are then averaged to summarize the population-level accessibility of plasmid mutations, which is then compared between the coculture and each monoculture (Mix – *E. coli;* Ec monoculture and Mix – *K. pneumoniae;* Kp monoculture). The positive Mix–Ec differences at low concentrations (0.03–0.125 μg/mL) reflect early collapse of low resistance genotypes (e.g., TEM-1) in *K. pneumoniae* subpopulation of the coculture, reducing Mix fitness of sensitive genotypes and enhancing the benefit of resistance mutations (E104K, R164S, G238S) compared to *E. coli* monoculture where resistance steps are not yet necessary (Fig. 4a).

Likewise, in 1-4 μg/mL CTX environments, the double mutant genotypes are inhibited in *K. pneumoniae* host but capable of growth in *E. coli* (Fig. 4b). Consequently, this genotype performs worse in coculture than it does in *E. coli* monoculture, but better in coculture than it does in *K. pneumoniae* monoculture. This pattern is replicated in when adding resistance mutations to more resistant backgrounds (Fig. 4c) where Mix-Ec is positive, but Mix-Kp is negative over the same intervals of concentration space. This space is where double mutants are inhibited in *K. pneumoniae* but persist in *E. coli* causing the fitness effect of resistance mutations to be more beneficial throughout these concentrations in coculture than they are in *E. coli* monoculture and to be less positive than they are in *K. pneumoniae* monoculture (Fig. 4c). Together, these patterns reveal that the fitness consequences of plasmid mutations are dynamically reshaped by ecological context, with distinct deformation signatures structured by species-specific resistance thresholds and competitive dynamics.

Discussion

Our results demonstrate that host community structure, in addition to host genetic background, plays a central role in shaping the adaptive window of plasmid-borne resistance mutations. Across monoculture and coculture experiments, we observe that the presence of a second species alters both the absolute fitness of plasmid genotypes and the relative fitness effects of individual mutations. These changes are structured by interspecific trade-offs in resistance and growth rate, which modulate the ecological setting in which selection on plasmid mutations occurs. As such, we find that the evolutionary accessibility of resistance mutations is not a fixed property of the genotype–environment pair, but a dynamic outcome of ecological competition and cooperative interactions between host species.

Chapters 1 and 2 reveal a fundamental ecological asymmetry between our focal hosts. In monoculture, *K. pneumoniae* exhibits a consistent growth and yield advantage, outcompeting *E. coli* across most of the cefotaxime gradient. Conversely, *E. coli* exhibits greater intrinsic resistance, persisting at high drug concentrations where *K. pneumoniae* is inhibited. These asymmetries carry over into coculture, where plasmid genotypes hosted by *K. pneumoniae* generally outperform those in *E. coli*—except at the highest drug concentrations, where ecological release of *E. coli* allows the more resistant species to dominate. Importantly, these competitive dynamics reshape not only which species carries the plasmid genotypes with highest fitness, but also which mutations are selectively favored at a given concentration.

In some cases, these dynamics lead to emergent eco-evolutionary interactions in coculture settings. At 32 µg/mL CTX, a concentration where *K. pneumoniae* monocultures are inhibited, the presence of *E. coli* enables *K. pneumoniae* to reach high densities via enzymatic degradation of cefotaxime. This case of interspecific protection involves a resistant species detoxifying the environment, thus enabling a sensitive competitor to grow through an alteration of the selective environment experienced by the host-plasmid pair. Such a scenario suggests the possibility of mutualistic eco-evolutionary dynamics: *K. pneumoniae* benefits from the presence of *E. coli*, while *E. coli* may gain access to beneficial plasmid mutations that do not yet possess a selective advantage to this more resistant species, but which are necessary in the that salvaged *K. pneumoniae* subpopulation.

To quantify the community-level reweighting of mutational effect, we calculated a deformation metric that measures the difference in fitness effect for a given mutation between monoculture and coculture settings (Figure 4). We find that coculture consistently shifts the accessibility of resistance mutations in opposite directions relative to each monoculture. For example, in low-drug environments, plasmid mutations are more beneficial in coculture than in *E. coli* monoculture (Mix–Ec > 0) due to early suppression of low-resistance genotypes in the *K. pneumoniae* subpopulation. However, the same mutations are less beneficial in coculture than in *K. pneumoniae* monoculture (Mix–Kp < 0), where growth rates are higher and resistance thresholds lower. This pattern reverses in high-drug environments, where *E. coli* survives alone but supports *K. pneumoniae* through detoxification. Here, *K. pneumoniae* experiences a relative increase in the benefit of resistance mutations, producing positive Mix–Kp deformation.

These results have important implications for our broader understanding of plasmid evolution. First, they highlight that plasmid adaptation is not merely a function of mutational input and antibiotic pressure but is shaped by the competitive and cooperative dynamics between hosts. Even when resistance effects are conserved across hosts, the net trajectory of plasmid evolution depends on which hosts dominate and under what conditions. This finding extends prior observations of host-specific adaptive windows and offers a putative mechanism of evolutionary "crowdsourcing"[58] across species wherein plasmids are driven to sample from a similar set of beneficial mutations in the host constrained most by environmental pressure.

Second, our results suggest that ecological and evolutionary processes act as coupled optimization problems unfolding on different scales.[63–65] Competitive dynamics determine which host species prevail under a given antibiotic regime, while selection acts within the plasmid population of each host to balance fitness and resistance trade-offs across mutationally adjacent genotypes. These processes are partially decoupled—plasmids are mobile and experience selection across hosts—but are nonetheless entangled through ecological feedback. The fitness effect of a plasmid mutation depends on its host, and the composition of host species is itself shaped by the consequences of plasmid evolution.

Finally, the framework we develop here may be applicable beyond antibiotic resistance. In microbial communities such as the gut microbiome, environmental microbiota, or engineered consortia, the evolution of mobile genes likely depends on both ecological context and genetic background. Shifts in species composition can open or close adaptive windows, alter selective gradients, and modulate the spread of resistance or other functional traits. Understanding these dynamics is crucial for both predictive microbiology and the rational design of multispecies systems. Future studies may expand this approach by incorporating temporal shifts in community structure, broader spectra of mutations, or explicit models of mobile element transfer. Nonetheless, the Chapter 2 demonstrates a fundamental principle: in systems where

fitness effects are context-dependent, the space of accessible evolutionary solutions is not fixed but reshaped by the interactions across levels of organization—from genes to genomes to communities.

Methods

Genetic Engineering

All *bla*$_{TEM}$ genotypes were engineered from the wildtype TEM-1 allele housed on a nonconjugative pBR322 plasmid vector using the Q5 site-directed mutagenesis kit with homemade aliquots of *E. coli* K12 (DH10B). In short, polymerase chain reaction with a Q5 DNA polymerase were performed with two "back-to-back" primers with the forward primer encoding the desired nucleotide change. PCR products were treated with the NEB Kinase, Ligase, and DpnI (KLD) kit. This kit facilitates the recircularization of the linear PCR product by phosphorylating (kinase) then fusing (ligase) the ends of the newly synthesized DNA molecule. KLD products will be transformed into homemade, chemically competent *E. coli* then Sanger sequenced (Azenta Biosciences) to ensure proper construction. Following confirmation, individual colonies with properly constructed alleles were used to initiate LB + 15 µg/mL cefotaxime cultures, grown overnight, then the plasmid was isolated using a Qiagen miniprep kit.

These plasmid minipreps were double-digested with NcoI-HF and NsiI-HF restriction endonucleases and treated with recombinant shrimp alkaline phosphatase to prevent recircularization of the vector. Separately, a barcoded insert molecule was constructed using a ~200 bp primer of which the interior contains a stretch of 18 unspecified (NNN) nucleotides. These single-stranded primers were filled in with the Klenow (exo-) fragment, then these insert oligonucleotides were digested with NcoI-HF and NsiI-HF and ligated into the linear vector using the T4 ligase enzyme downstream of the *bla*$_{TEM}$ coding DNA sequence in the modified pBR322 vector backbone. Ligated product was transformed into 100 µL aliquots of homemade chemically competent *E. coli.* Barcode sequences for all isolates were identified via Sanger sequencing and the full gene plus barcode region was sequenced for one replicate per genotype.

Barcoded Monoculture MIC Experiment

Plasmid genotypes were barcoded in triplicate and one barcoded replicate of these additional genotypes were added to three separate plasmid libraries: Lib I, II, III. Plasmid libraries were processed using the Zymo Clean and Concentrator Kit then individually transformed into three 100 µL aliquots of homemade electrocompetent cells of *E. coli* and *K. pneumoniae* using a Gene Pulser apparatus with a field strength of 2.5 kV and a time constant of ~6 ms. Competent cells were resuspended in 950 µL LB, transferred to 1.7 mL microcentrifuge tubes (Eppendorf), and recovered at 37 ˚C with shaking for 1 hour. Transformant library size was estimated via plating on LB agar + 15 µg/mL tetracycline and 800 µL of the library was used to inoculate six (Lib I, II, III in *E. coli* and *K. pneumoniae*) LB + 15 µg/mL tetracycline (final concentration) cultures grown overnight.

Following overnight growth, cultures were pelleted and resuspended in 4 mL and 8 mL, respectively, to account for differences in yield between species. Monoculture and coculture libraries were prepared and diluted into Mueller-Hinton broth. Cultures were inoculated along a two-fold cefotaxime gradient prepared from serial dilutions of a 41 mg/mL stock solution, with starting densities targeting ~5×10^5 CFU/mL. Cultures were incubated at 37 °C with shaking and sampled for density and barcode frequencies at 0, 5, and 20 hours. Bacterial densities were estimated via selective plating (LB + 15 µg/mL tetracycline for plasmid-contained cells, LB +

100 µg/mL streptomycin for *E. coli*, and Koser Citrate for *K. pneumoniae*) and barcode frequencies were quantified using culture PCR followed by short-read amplicon sequencing of the barcode region (Azenta Biosciences).

Fitness Analysis

Plasmid genotype frequencies were estimated by proxy through short-read amplicon sequencing of the associated barcode region. Cell pellets were thawed from -20 ˚C and 1 µL of this cell suspension was used as template in a culture PCR with Q5 DNA polymerase and primers bearing partial Illumina adapters. Each experimental sample was individually amplified, cleaned, normalized to 20 ng/µL, and submitted for EZ amplicon sequencing by Azenta Biosciences. Barcode-level growth rates were calculated as:

$$r_{i,c,s} = \frac{1}{20}\left\{\ln\frac{f_{i,c,s}(20)D_{c,s}(20)}{f_{i,c,s}(0)D_{c,s}(0)}\right\}$$

where $f_{i,c,s}(t)$ denotes the frequency of the i^{th} barcode in media with a drug concentration of c in species s at time t and $D_{c,s}(t)$ is the total culture density of species s in media with a drug concentration of c at time t . Genotypic growth rates were computed as the mean of all barcoded replicates within the same antibiotic concentration and species (i.e., averaging $r_{i,c,s}$ over the relevant i values while fixing c and s). More technically, suppose the set of barcodes corresponding to genotype g is given as $\mathbf{B}_g$, then we have the mean growth rate of this genotype

$$\bar{r}_{g,c,s} = \frac{1}{|\mathbf{B}_g|}\sum_{i\in\mathbf{B}_g} r_{i,c,s}$$

To represent statistical uncertainty around plasmid genotype fitness estimates, 95% confidence intervals (CIs) were computed for each genotype across antibiotic concentrations and species, a representative set is shown in Figure 3. For each genotype (g), drug concentration (c), and species (s), the standard error of the mean growth rate was calculated from the set of barcode replicates

$$SE_{g,c,s} = \frac{SD([r(i,c,s): i \in \mathbf{B}_g}{\sqrt{|\mathbf{B}_g|}}$$

where SD denotes the standard deviation of barcode-level growth rates. The 95% confidence interval around the mean growth rate was then defined as:

$\text{CI95\%} = \bar{r}_{g,c,s} \pm 1.96 \times SE_{g,c,s}$

Two independently prepared and sequenced $t = 0$ samples for each species were used to confirm consistency in the initial distribution of genotypes prior to selection across the cefotaxime gradient. Following a log10 transformation, initial barcode frequencies exhibited high

concordance between replicates in both species (Pearson correlation coefficient 0.99 in *E. coli* and 0.99 in *K. pneumoniae* in pairwise comparisons between replicates).

Calculation of Plasmid Mutational Effect and Community Deformation Metric

To quantify how plasmid mutation effects vary across ecological contexts, we calculated the relative fitness difference [(Mutant Fitness – Ancestor Fitness / Mutant Fitness)] as in Chapter 1 between mutant neighbor genotypes within the same barcode type in both monoculture and coculture treatments. Mutational neighbors were identified based on string comparison of genotype names (e.g., TEM-1 → E104K) and fitness difference was computed as the scaled relative difference in barcode-specific growth rate between the mutant and original genotypes within each host species barcode type (*E. coli* only, *K. pneumoniae* only, and hybrid) and antibiotic concentration. In monoculture, fitness effects were calculated between the mutant and original genotypes within each host species barcode type (i.e., pseudo-replicates within the monoculture communities) and antibiotic concentration.

To assess ecological deformation of these mutational fitness effects, we calculated the difference in mutational effect between coculture and monocultures of each species within each tested concentration: $\Delta\Delta Fitness$ = Relative Fitness Difference in Mix – Relative Fitness Difference in *E. coli* Monoculture and $\Delta\Delta Fitness$ = Relative Fitness Difference in Mix – Relative Fitness Difference in *K. pneumoniae* Monoculture. Positive $\Delta\Delta Fitness$ values indicate that the mutation conferred a greater mean fitness difference in coculture community than in the compared monoculture; negative values indicate the opposite. These deformation scores plotted as a function of antibiotic concentration to identify regions where community context amplified or suppressed the fitness effect of resistance mutations in Figure 4.

Bibliography

1. Baquero F, Martínez JL, F. Lanza V, Rodríguez-Beltrán J, Galán JC, San Millán A, et al. Evolutionary Pathways and Trajectories in Antibiotic Resistance. Clin Microbiol Rev. 2021 Jun 30;34(4):e00050-19.

2. Cano AV, Gitschlag BL, Rozhoňová H, Stoltzfus A, McCandlish DM, Payne JL. Mutation bias and the predictability of evolution. Philos Trans R Soc B Biol Sci. 378(1877):20220055.

3. Firnberg E, Labonte JW, Gray JJ, Ostermeier M. A Comprehensive, High-Resolution Map of a Gene's Fitness Landscape. Mol Biol Evol. 2014 Jun;31(6):1581–92.

4. Gillespie JH. Molecular Evolution Over the Mutational Landscape. Evolution. 1984;38(5):1116–29.

5. Gillespie JH, Turelli M. Genotype-environment interactions and the maintenance of polygenic variation. Genetics. 1989 Jan;121(1):129–38.

6. Hietpas RT, Bank C, Jensen JD, Bolon DNA. Shifting fitness landscapes in response to altered environments. Evol Int J Org Evol. 2013 Dec;67(12):10.1111/evo.12207.

7. Johnson MS, Reddy G, Desai MM. Epistasis and evolution: recent advances and an outlook for prediction. BMC Biol. 2023 May 24;21(1):120.

8. Ascensao JA, Wetmore KM, Good BH, Arkin AP, Hallatschek O. Quantifying the local adaptive landscape of a nascent bacterial community. Nat Commun. 2023 Jan 16;14(1):248.

9. Das SG, Direito SO, Waclaw B, Allen RJ, Krug J. Predictable properties of fitness landscapes induced by adaptational tradeoffs. eLife. 2020 May 19;9:e55155.

10. Diaz-Colunga J, Skwara A, Vila JCC, Bajic D, Sanchez A. Global epistasis and the emergence of function in microbial consortia. Cell. 2024 Jun 6;187(12):3108-3119.e30.

11. Fiegna F, Moreno-Letelier A, Bell T, Barraclough TG. Evolution of species interactions determines microbial community productivity in new environments. ISME J. 2015 May;9(5):1235–45.

12. Gorter FA, Manhart M, Ackermann M. Understanding the evolution of interspecies interactions in microbial communities. Philos Trans R Soc B Biol Sci. 2020 Mar 23;375(1798):20190256.

13. Gupta A, Zaman L, Strobel HM, Gallie J, Burmeister AR, Kerr B, et al. Host-parasite coevolution promotes innovation through deformations in fitness landscapes. Ogbunugafor CB, Walczak AM, Barr J, editors. eLife. 2022 Jul 6;11:e76162.

14. Hart SFM, Chen CC, Shou W. Pleiotropic mutations can rapidly evolve to directly benefit self and cooperative partner despite unfavorable conditions. Verstrepen KJ, Tautz D, editors. eLife. 2021 Jan 27;10:e57838.

15. Letten AD, Hall AR, Levine JM. Using ecological coexistence theory to understand antibiotic resistance and microbial competition. Nat Ecol Evol. 2021 Apr;5(4):431–41.

16. Meyer B, Kuehl JV, Deutschbauer AM, Arkin AP, Stahl DA. Flexibility of syntrophic enzyme systems in Desulfovibrio species ensures their adaptation capability to environmental changes. J Bacteriol. 2013 Nov;195(21):4900–14.

17. Pacheco AR, Osborne ML, Segrè D. Non-additive microbial community responses to environmental complexity. Nat Commun. 2021 Apr 22;12(1):2365.

18. Sanz-García F, Gil-Gil T, Laborda P, Blanco P, Ochoa-Sánchez LE, Baquero F, et al. Translating eco-evolutionary biology into therapy to tackle antibiotic resistance. Nat Rev Microbiol [Internet]. 2023 May 19 [cited 2023 Jul 20]; Available from: https://www.nature.com/articles/s41579-023-00902-5

19. Sørensen MES, Wood AJ, Cameron DD, Brockhurst MA. Rapid compensatory evolution can rescue low fitness symbioses following partner switching. Curr Biol. 2021 Sep 13;31(17):3721-3728.e4.

20. Venkataram S, Kuo HY, Hom EFY, Kryazhimskiy S. Mutualism-enhancing mutations dominate early adaptation in a two-species microbial community. Nat Ecol Evol. 2023 Jan;7(1):143–54.

21. Wade MJ. The co-evolutionary genetics of ecological communities. Nat Rev Genet. 2007 Mar;8(3):185–95.

22. Zomorrodi AR, Segrè D. Genome-driven evolutionary game theory helps understand the rise of metabolic interdependencies in microbial communities. Nat Commun. 2017 Nov 16;8(1):1563.

23. Breen MS, Kemena C, Vlasov PK, Notredame C, Kondrashov FA. Epistasis as the primary factor in molecular evolution. Nature. 2012 Oct 25;490(7421):535–8.

24. Burmeister AR, Lenski RE, Meyer JR. Host coevolution alters the adaptive landscape of a virus. Proc R Soc B Biol Sci. 2016 Sep 28;283(1839):20161528.

25. Conlin PL, Chandler JR, Kerr B. Games of life and death: antibiotic resistance and production through the lens of evolutionary game theory. Curr Opin Microbiol. 2014 Oct;21:35–44.

26. Diaz-Colunga J, Sanchez A, Ogbunugafor CB. Environmental modulation of global epistasis in a drug resistance fitness landscape. Nat Commun. 2023 Dec 5;14:8055.

27. Farahpour F, Saeedghalati M, Brauer VS, Hoffmann D. Trade-off shapes diversity in eco-evolutionary dynamics. Doebeli M, Baldwin IT, Ispolatov Y, editors. eLife. 2018 Aug 17;7:e36273.

28. Knopp M, Andersson DI. Predictable Phenotypes of Antibiotic Resistance Mutations. mBio. 2018 May 15;9(3):10.1128/mbio.00770-18.

29. Laland K, Matthews B, Feldman MW. An introduction to niche construction theory. Evol Ecol. 2016 Apr 1;30(2):191–202.

30. Lambert G, Vyawahare S, Austin RH. Bacteria and game theory: the rise and fall of cooperation in spatially heterogeneous environments. Interface Focus. 2014 Aug 6;4(4):20140029.

31. Lindsey HA, Gallie J, Taylor S, Kerr B. Evolutionary rescue from extinction is contingent on a lower rate of environmental change. Nature. 2013 Feb;494(7438):463–7.

32. Mehlhoff JD, Stearns FW, Rohm D, Wang B, Tsou EY, Dutta N, et al. Collateral fitness effects of mutations. Proc Natl Acad Sci. 2020 May 26;117(21):11597–607.

33. Ogbunugafor CB. The mutation effect reaction norm (mu-rn) highlights environmentally dependent mutation effects and epistatic interactions. Evolution. 2022 Feb 1;76(s1):37–48.

34. Roca CP, Cuesta JA, Sánchez A. Evolutionary game theory: Temporal and spatial effects beyond replicator dynamics. Phys Life Rev. 2009 Dec 1;6(4):208–49.

35. Ruelens P, de Visser JAGM. Choice of β-Lactam Resistance Pathway Depends Critically on Initial Antibiotic Concentration. Antimicrob Agents Chemother. 65(8):e00471-21.

36. Schenk MF, Szendro IG, Salverda MLM, Krug J, De Visser JAGM. Patterns of Epistasis between Beneficial Mutations in an Antibiotic Resistance Gene. Mol Biol Evol. 2013 Aug;30(8):1779–87.

37. Scheuerl T, Hopkins M, Nowell RW, Rivett DW, Barraclough TG, Bell T. Bacterial adaptation is constrained in complex communities. Nat Commun. 2020 Feb 6;11(1):754.

38. Watson RA, Ebner M. Eco-Evolutionary Dynamics on Deformable Fitness Landscapes. In: Richter H, Engelbrecht A, editors. Recent Advances in the Theory and Application of Fitness Landscapes [Internet]. Berlin, Heidelberg: Springer Berlin Heidelberg; 2014 [cited 2023 Sep 6]. p. 339–68. (Emergence, Complexity and Computation; vol. 6). Available from: https://link.springer.com/10.1007/978-3-642-41888-4_12

39. Wortel MT, Agashe D, Bailey SF, Bank C, Bisschop K, Blankers T, et al. Towards evolutionary predictions: Current promises and challenges. Evol Appl. 2023 Jan;16(1):3–21.

40. Xie VC, Pu J, Metzger BP, Thornton JW, Dickinson BC. Contingency and chance erase necessity in the experimental evolution of ancestral proteins. Courtier-Orgogozo V, Przeworski M, Courtier-Orgogozo V, Blount ZD, editors. eLife. 2021 Jun 1;10:e67336.

41. Benz F, Hall AR. Host-specific plasmid evolution explains the variable spread of clinical antibiotic-resistance plasmids. Proc Natl Acad Sci. 2023 Apr 11;120(15):e2212147120.

42. Doi Y, Adams-Haduch JM, Peleg AY, D'Agata EM. The role of horizontal gene transfer in the dissemination of extended-spectrum beta-lactamase-producing Escherichia coli and Klebsiella pneumoniae isolates in an endemic setting. Diagn Microbiol Infect Dis. 2012 Sep;74(1):34–8.

43. Gama JA, Kloos J, Johnsen PJ, Samuelsen Ø. Host dependent maintenance of a blaNDM-1-encoding plasmid in clinical Escherichia coli isolates. Sci Rep. 2020 Jun 9;10(1):9332.

44. Jordt H, Stalder T, Kosterlitz O, Ponciano JM, Top EM, Kerr B. Coevolution of host–plasmid pairs facilitates the emergence of novel multidrug resistance. Nat Ecol Evol. 2020 Jun;4(6):863–9.

45. Lee IPA, Eldakar OT, Gogarten JP, Andam CP. Bacterial cooperation through horizontal gene transfer. Trends Ecol Evol. 2022 Mar 1;37(3):223–32.

46. Lerminiaux NA, Cameron ADS. Horizontal transfer of antibiotic resistance genes in clinical environments. Can J Microbiol. 2019 Jan;65(1):34–44.

47. Loftie-Eaton W, Bashford K, Quinn H, Dong K, Millstein J, Hunter S, et al. Compensatory mutations improve general permissiveness to antibiotic resistance plasmids. Nat Ecol Evol. 2017 Sep;1(9):1354–63.

48. Bottery MJ. Ecological dynamics of plasmid transfer and persistence in microbial communities. Curr Opin Microbiol. 2022 Aug 1;68:102152.

49. Brockhurst MA, Harrison E. Ecological and evolutionary solutions to the plasmid paradox. Trends Microbiol. 2022 Jun 1;30(6):534–43.

50. Vogwill T, MacLean RC. The genetic basis of the fitness costs of antimicrobial resistance: a meta-analysis approach. Evol Appl. 2015 Mar;8(3):284–95.

51. Wyres KL, Holt KE. Klebsiella pneumoniae as a key trafficker of drug resistance genes from environmental to clinically important bacteria. Curr Opin Microbiol. 2018 Oct;45:131–9.

52. Amanatidou E, Matthews AC, Kuhlicke U, Neu TR, McEvoy JP, Raymond B. Biofilms facilitate cheating and social exploitation of β-lactam resistance in Escherichia coli. Npj Biofilms Microbiomes. 2019 Nov 29;5(1):1–10.

53. Artemova T, Gerardin Y, Dudley C, Vega NM, Gore J. Isolated cell behavior drives the evolution of antibiotic resistance. Mol Syst Biol. 2015 Jul;11(7):822.

54. Dugatkin LA, Perlin M, Lucas JS, Atlas R. Group-beneficial traits, frequency-dependent selection and genotypic diversity: an antibiotic resistance paradigm. Proc Biol Sci. 2005 Jan 7;272(1558):79–83.

55. Perlin MH, Clark DR, McKenzie C, Patel H, Jackson N, Kormanik C, et al. Protection of Salmonella by ampicillin-resistant Escherichia coli in the presence of otherwise lethal drug concentrations. Proc Biol Sci. 2009 Nov 7;276(1674):3759–68.

56. Schenk MF, Zwart MP, Hwang S, Ruelens P, Severing E, Krug J, et al. Population size mediates the contribution of high-rate and large-benefit mutations to parallel evolution. Nat Ecol Evol. 2022 Mar 3;6(4):439–47.

57. Levin SR, Gandon S, West SA. The social coevolution hypothesis for the origin of enzymatic cooperation. Nat Ecol Evol. 2020 Jan;4(1):132–7.

58. Kosterlitz O, Grassi N, Werner B, McGee RS, Top EM, Kerr B. Evolutionary crowdsourcing: alignment of fitness landscapes allows cross-species adaptation of a horizontally transferred gene [Internet]. Evolutionary Biology; 2022 Sep [cited 2023 Jan 29]. Available from: http://biorxiv.org/lookup/doi/10.1101/2022.09.13.507827

59. Negri MC, Lipsitch M, Levin BR, Baquero F. Concentration-Dependent Selection of Small Phenotypic Differences in TEM ᴺʟ-Lactamase-Mediated Antibiotic Resistance. ANTIMICROB AGENTS CHEMOTHER. 2000;44.

60. Palzkill T. Structural and Mechanistic Basis for Extended-Spectrum Drug-Resistance Mutations in Altering the Specificity of TEM, CTX-M, and KPC β-lactamases. Front Mol Biosci. 2018 Feb 23;5:16.

61. Salverda MLM, Dellus E, Gorter FA, Debets AJM, Oost J van der, Hoekstra RF, et al. Initial Mutations Direct Alternative Pathways of Protein Evolution. PLOS Genet. 2011 Mar 3;7(3):e1001321.

62. Salverda MLM, De Visser JAGM, Barlow M. Natural evolution of TEM-1 β-lactamase: experimental reconstruction and clinical relevance. FEMS Microbiol Rev. 2010 Nov 1;34(6):1015–36.

63. Levin M. Darwin's agential materials: evolutionary implications of multiscale competency in developmental biology. Cell Mol Life Sci CMLS. 2023 May 8;80(6):142.

64. Shreesha L, Levin M. Cellular Competency during Development Alters Evolutionary Dynamics in an Artificial Embryogeny Model. Entropy. 2023 Jan;25(1):131.

65. Hartl B, Risi S, Levin M. Evolutionary Implications of Self-Assembling Cybernetic Materials with Collective Problem-Solving Intelligence at Multiple Scales. Entropy. 2024 Jul;26(7):532.